



**MODELLING OF THERMOMAGNETIC GENERATOR BASED
ON MAGNETIC AND THERMODYNAMIC PROPERTIES OF
GADOLINIUM**

Bachelor's Thesis

Student: Mihhail Olentšenko

Student code: 213498YAFB

Supervisor: Jaan Kalda, Prof., TalTech, Department of Cybernetics

Programme: Applied Physics

Tallinn 2024



**TERMOMAGNETILISE GENERAATORI MODELEERUMINE
GADOLIINIUMI MAGNETILISTE JA TERMODÜNAAMILISTE
OMADUSTE PÕHJAL**

Bakalaureusetöö

Üliõpilane: Mihhail Olentšenko

Üliõpilaskood: 213498YAFB

Juhendaja: Jaan Kalda, Prof., TalTech, Küberneetika instituut

Õppekava: Rakendusfüüsika

Tallinn 2024

Author's Declaration of Originality

I hereby declare that I have written this thesis independently and the thesis has not previously been submitted for defence. All works and major viewpoints of the other authors, data from sources of literature and elsewhere used for writing this paper have been properly cited.

Author: Mihhail Olentšenko

20.05.2024

The thesis complies with the requirements for bachelor's/master's theses.

Supervisor: Jaan Kalda

20.05.2024

The non-exclusive license for reproduction and publication of a graduation thesis is included in appendix 1.

Table of Contents

Introduction	3
1 Theoretical Framework	5
1.1 Numerical Methods	5
1.2 Gadolinium Properties	6
1.3 Thermodynamic Processes	6
1.4 Magnetic Field Distribution	9
1.5 Electricity Generation	14
2 Data Preparation	17
2.1 Acquisition	17
2.2 Interpolation	17
2.3 Validation	18
3 Generator Simulation	21
3.1 Magnetic Field Distribution	21
3.2 Thermodynamic Processes	22
3.3 Electricity Generation	23
3.4 Simulation	25
3.5 Visualization of Results	26
4 Results	27
4.1 Triple Gadolinium Bar Simulation Results	27
4.2 Series Simulation Results	31
4.3 Optimization of Parameters	33
4.4 Optimization of Geometry	39
4.5 Analysis of Optimal Conditions	41
4.6 Results in Optimal Conditions	46
5 Conclusions	48
5.1 Equations	48
5.2 Gadolinium Properties	48
5.3 Magnetic Field Distribution	49
5.4 Magnetocaloric Effect	51
5.5 Evaluation of the Model	52

Acknowledgements	53
References	54
Abstract	56
Annotatsioon	57
Appendices	58
Appendix 1 – Non-Exclusive License for Reproduction and Publication of a Graduation Thesis	58
Appendix 2 – Extracted Data and Simulation Code	59

Introduction

It is well established that electrical energy is one of the cornerstones of modern civilization. Currently, there is a multitude of electricity production methods in use, ranging from fossil fuel energy production to nuclear and green energy. Many methods have immediate negative consequences, such as waste products being released into the surroundings, and long-term negative consequences, the most alarming of which is climate change. To negate or at least minimize these problems, a large effort is being made to transition to electricity production methods known as green energy.

Like all methods, green energy has its drawbacks. Output energy inconsistency is one of them: production rate changes greatly seasonally and daily, and often these changes can be unpredictable. Accounting for these variations is not a trivial task: large-scale energy storage is problematic due to high costs and land use. Moreover, if energy production or storage is distributed over a large area, there is a need to create a distribution network, which is limited by energy loss in power lines.

Most green energy production methods are based on natural or artificial heat exchange processes. Geothermal energy is acquired from the Earth's hot core, solar energy is received from heat radiated from the sun, and winds and currents are a result of convective heat exchange in the atmosphere and hydrosphere. However, direct production of energy from a temperature gradient is more complex. [1]

Often mechanical methods are used, where heat energy is transformed into mechanical energy, either artificially or naturally. These methods require large temperature gradients to produce meaningful amounts of electricity. A large portion of energy is used to compensate for mechanical losses.

Since a lot of waste heat is dissipated into the environment but the temperature gradients in these cases are usually small, **a generator that works from a small thermal gradient near room temperature would allow the consumption of this potential energy** [2]. Although the thermoelectric effect is theoretically an efficient solution at low temperature gradients, the real efficiency is limited by parasitic heat transfer in the conductive wires. For high efficiency, the wires would need to be good electrical conductors and good thermal insulators simultaneously, which are fundamentally contradictory requirements.

Another potentially applicable method is based on temperature oscillation around the Curie temperature of a ferromagnetic material. Since at this temperature point, the magnetic permeability of a ferromagnetic material changes drastically, it is possible to achieve a large

magnetic flux change, which results in electric field generation. Another benefit of working with a magnetic field is that the cold and hot parts of the generator can be properly isolated, unlike in the case of a thermoelectric generator.

Most ferromagnetic materials have their Curie temperature outside of reasonable bounds for generation. There is a notable exception: the rare-earth metal gadolinium (${}_{64}\text{Gd}$). Curie temperature of this metal is $T_{\text{Curie}} = 295 \text{ K} = 22^\circ\text{C}$, which is close to room temperature [3].

Gadolinium magnetic properties have been extensively researched and documented in the past hundred years [4, 5, 6]. Technological development has allowed the research of properties in more extreme cases, for example, at a microscopic scale [7, 8], or in strong magnetic fields [9]. These unique properties are being used for purposes of magnetic refrigeration and electrical power generation [10, 11].

The concept of using a gadolinium-based thermomagnetic generator has been demonstrated as a viable approach; however, its practical application is only now becoming feasible [12, 13]. The development in precise processing of materials has allowed higher efficiency [14]. As a result, high performance thermomagnetic near-room-temperature generator concepts and designs with novel refinements, such as latent heat transfer, are being developed and introduced [15, 16, 17]. Increased computing power has allowed the feasible simulation of magnetic field distribution and thermodynamic processes, which is an important preparatory step before beginning construction of a physical model [18].

The main goal of this thesis is to develop a numerical model of a thermomagnetic generator based on the phase transition of gadolinium. This model will be used as a tool for finding the optimal set of parameters for such a generator. The process of achieving this goal is divided into several steps. The first step is to build the theoretical framework for the numerical simulations. This includes deriving the required formulae, describing the generator in equations, making reasonable approximations to simplify this set of equations, and developing suitable numerical integration methods. The second step is to describe the properties of gadolinium numerically, using results from existing research papers. The final step is to test the numerical method with realistic input parameters.

1. Theoretical Framework

In this chapter, theoretical basis for the simulation is described. This includes equations and solution methods, which are later realized in simulation code.

1.1 Numerical Methods

In order to calculate the output of a generator based on magnetic and thermodynamic properties of gadolinium, the following properties must be quantified at different temperatures and magnetic field values: heat capacity of gadolinium $C(\vec{B}, T, \nu_{\text{Gd}})$, magnetization of gadolinium $\vec{M}(\vec{B}, T)$, and temperature differential due to magnetocaloric effect $dT(\vec{B}, T, d\vec{B})$.¹ In this thesis, the 1998 article "Magnetic phase transitions and the magnetothermal properties of gadolinium" by Dan'kov, Tishin, Pecharsky and Gschneidner was used as a source of the properties of gadolinium [6].

From electromagnetism [19] it is known, that $\mathcal{E} \equiv \oint_L \vec{E} \cdot d\vec{l} = -\frac{d\Phi_B}{dt}$, where \mathcal{E} is electromotive force and Φ_B is magnetic field flux through closed contour L . Magnetic field flux Φ_B through gadolinium changes due to temperature change of gadolinium and consequent change of its magnetic properties. Invoking heat-temperature equation $dQ = C(B, T, \nu_{\text{Gd}})dT$ and heat flux equation $W \equiv \frac{dQ}{dt} = \frac{\kappa A \Delta T}{l} \equiv K(T_0 - T)$, the following equation can be derived:

$$C(B, T, \nu_{\text{Gd}})dT = K(T_0 - T)dt. \quad (1.1)$$

This is the main differential equation that has to be solved.² Since heat capacity C and magnetic field B themselves are functions of temperature, the equation becomes more complex. Additionally, these dependencies are not described by simple functions, but are taken from measurements and interpolated. Therefore, it is reasonable to use numerical methods to solve this equation for the purposes of this thesis. The Euler method will be used for the solution, unless it is proven to be insufficiently accurate.

Since the application of numerical methods is practically impossible by hand, a computer code will be utilized. The *Python* programming language has been selected for this purpose [20]. Additionally, libraries *NumPy* [21], *pandas* [22] [23], *SciPy* [24] and *Matplotlib* [25] are used for specific purposes as described in chapters 2 and 3.

¹Further it can be seen, that using magnetic field in vector form is not required, therefore scalar form will be used from this point.

²Here, the derivation of the above equations is done very briefly, to introduce complications early on. For more in-depth look at the theoretical basis see further subsections.

1.2 Gadolinium Properties

Firstly, the magnetic properties of gadolinium must be defined. Magnetic field strength is defined as $\vec{H} = \frac{\vec{B}}{\mu_0} - \vec{M}$, where magnetization is $\vec{M}(\vec{B}, T)$. For gadolinium, measured magnetization data M_{data} is used [6]. Here, magnetization unit $[M_{\text{data}}] = \frac{\text{emu}}{\text{g}} = \frac{\text{erg}}{\text{G}\cdot\text{g}} = \frac{10^{-7}\text{J}}{10^{-4}\cdot 10^{-3}\text{T}\cdot\text{kg}} = \frac{\text{J}}{\text{T}\cdot\text{kg}} = \frac{\text{m}^2\cdot\text{A}}{\text{kg}}$, which is the SI unit for mass magnetization. Volume magnetization is required:

$$M = \frac{m}{V}M_{\text{data}} = \rho M_{\text{data}}, \quad (1.2)$$

where ρ is gadolinium density. Therefore, magnetization unit $[M] = \frac{\text{A}}{\text{m}}$. In the paper [6], magnetization measurements are provided for two crystal lattice directions. Since the generator is a macroscopic object, crystal lattice directions can be assumed to be randomly distributed. Therefore, it is reasonable to take an average value.

Secondly, the heat capacitance of gadolinium has to be defined. Again, molar heat capacitance $c_\nu(B, T)$ is taken from measured data [6]. Here, molar heat capacitance unit $[c_\nu] = \frac{\text{J}}{\text{mol}\cdot\text{K}}$. It would be more convenient to use volume heat capacitance in further calculations, thus:

$$\begin{aligned} c_m &= \frac{\nu}{m}c_\nu = \frac{1}{\mu}c_\nu, \\ c_V &= \frac{m}{V}c_m = \rho c_m = \frac{\rho}{\mu}c_\nu, \end{aligned} \quad (1.3)$$

where μ is molar mass and ρ is density. Then, volume heat capacitance unit $[c_V] = \frac{\text{J}}{\text{m}^3\cdot\text{K}}$.

Thirdly, temperature change due to magnetocaloric effect can be used to test the calculations and interpolated data. Measured magnetocaloric effect ΔT can be used for this purpose [6]. The validation of data, interpolated for the purpose of this thesis, is done in chapter 2.

Finally, gadolinium density and molar mass are required for the above equations. They can be acquired from an online database: $\rho = 7900 \text{ kg/m}^3$ and $\mu = 157.25 \text{ g/mol}$ [26].

1.3 Thermodynamic Processes

First and foremost, generator configuration has to be defined. In this thesis, configurations are based on the ones introduced in 2019 article "Energy harvesting near room temperature using a thermomagnetic generator with a pretzel-like magnetic flux topology" by Anja Waske, Daniel Dzekan, Kai Sellschopp, Dietmar Berger, Alexander Stork, Kornelius Nielsch and Sebastian Fähler [15].

First configuration for the simulation consists of two rectangular ferromagnetic plates, between far ends of which a permanent magnet and gadolinium bar are placed (see figure 1). Second configuration consists of two rectangular ferromagnetic plates, between the center areas of

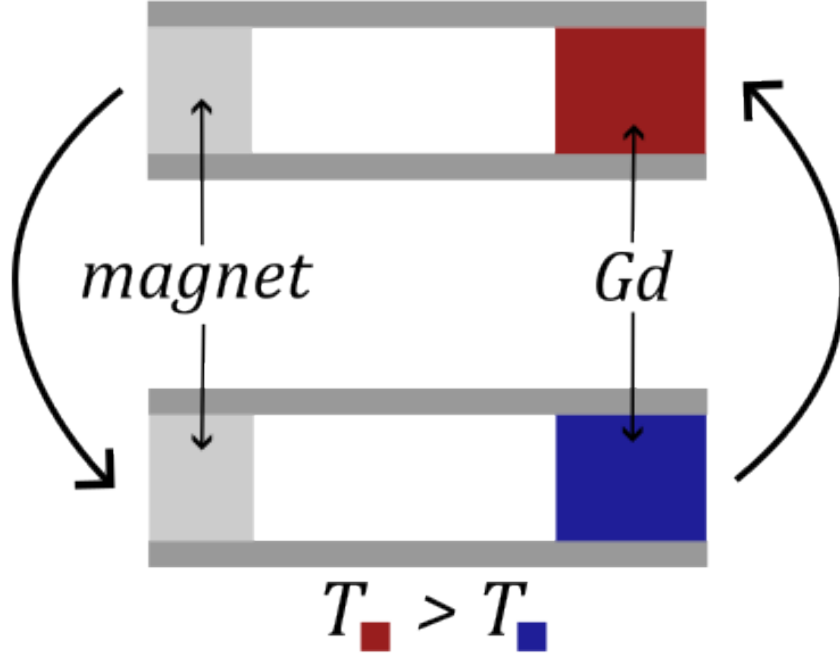


Figure 1. Single gadolinium bar configuration

which a permanent magnet is placed, and between the far ends two gadolinium bars are placed; the phase shift between temperatures is 180° (see figure 2). Third configuration consists of two triangular-like ferromagnetic plates, between the center areas of which a permanent magnet is placed, and between the far ends three gadolinium bars are placed; the phase shift between temperatures is 120° . In every case the generator coils are placed around the gadolinium bars.³

It can be assumed that gadolinium temperature perturbations within the bar are negligible (so that the temperature of gadolinium bars is considered homogeneous). Additionally, heat flux $W \equiv \frac{dQ}{dt}$ only occurs between designated heaters/coolers to/from gadolinium bars and no heat escapes to ferromagnetic plates or air. The heat flux is distributed equally in gadolinium, so that temperature stays homogeneous.

Change of temperature is achieved by directing liquid currents through heat exchangers. This liquid has some known temperature T_{liquid} , the heat exchanger has known heat transfer parameter $K \equiv \frac{\kappa A}{l}$, where κ is thermal conductivity of the pipe material, A is pipe contact area with gadolinium, and l is pipe wall thickness. Then, heat flux from heat exchanger to gadolinium with temperature T :

$$\frac{dQ}{dt} = K(T_{\text{liquid}} - T). \quad (1.4)$$

³In third configuration, two generators can work in tandem to produce three-phase electric power with non-stop flow of both liquids, which is why this configuration was introduced in addition to described in research [15].

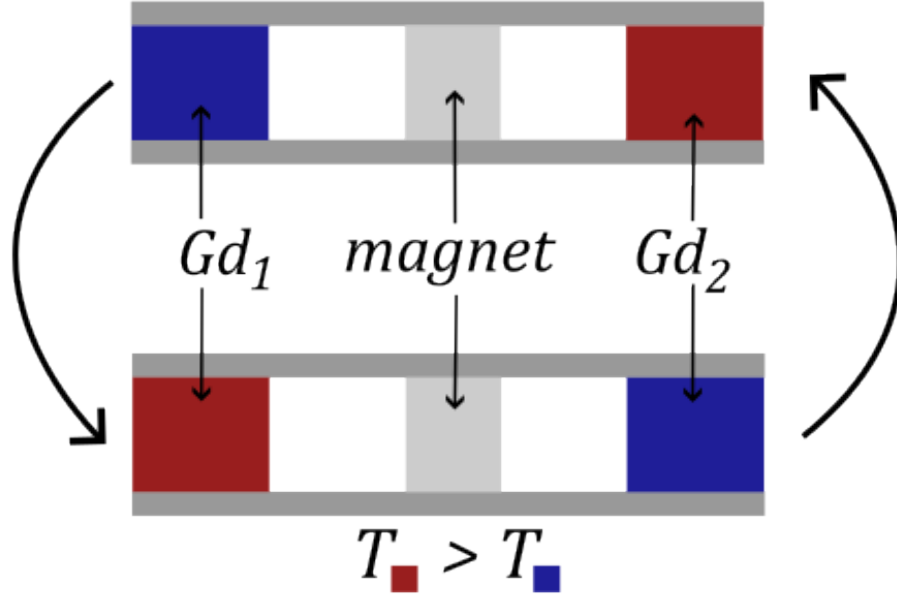


Figure 2. Double gadolinium bar configuration

It is known from thermodynamics [27], that heat dQ transferred from heat exchanger to gadolinium bar in time dt changes gadolinium bar temperature by dT according to the following law:

$$dQ = c_V V_{Gd} dT, \quad (1.5)$$

where V_{Gd} is gadolinium bar volume, and c_V is volume heat capacitance of gadolinium from equation 1.3. Substitution of dQ from equation 1.4 can be made:

$$c_V V_{Gd} dT = K(T_{liquid} - T)dt. \quad (1.6)$$

Operating under assumption that c_V is constant, we can solve this differential equation:⁴

$$\begin{aligned} \frac{dT}{T_{liquid} - T} &= \frac{K dt}{c_V V_{Gd}}, \\ \int \frac{dT}{T_{liquid} - T} &= \int \frac{K dt}{c_V V_{Gd}}, \\ \ln(T_{liquid} - T) &= -\frac{K}{c_V V_{Gd}} t + \ln(T_{liquid} - T_0) \\ T_{liquid} - T &= (T_{liquid} - T_0) e^{-\frac{K}{c_V V_{Gd}} t}, \\ T &= T_{liquid} - (T_{liquid} - T_0) e^{-\frac{K}{c_V V_{Gd}} t}. \end{aligned} \quad (1.7)$$

Here, T_0 is initial gadolinium temperature. Hence, it can be seen that gadolinium temperature T approaches liquid temperature T_{liquid} exponentially with time. Therefore $t \rightarrow +\infty \Rightarrow T \rightarrow T_1$.

⁴Here, $\ln(T_{liquid} - T_0)$ is an integration constant.

In order to achieve electricity generation, gadolinium temperature has to change. The obvious way to achieve this is to change the "target" temperature T_{liquid} from cold $T_{\text{liquid,C}}$ to hot $T_{\text{liquid,H}}$ and back to cold $T_{\text{liquid,C}}$ with some frequency f_{liquid} . These parameters have to be optimized.

For simplification reasons, it will be assumed, that liquid effective heat capacity is infinite (it has constant temperature in the heat exchanger), and that switch between hot and cold liquids is instantaneous. First condition can be achieved by providing sufficiently fast flow rate through the heat exchanger.

Additionally, one must not forget, that gadolinium heat capacitance c_V is dependent on magnetic induction B and temperature T , so equation 1.7 can only be used as a first approximation of the process.

1.4 Magnetic Field Distribution

To generate electricity, magnetic field flux has to change:

$$\mathcal{E} \equiv \oint_L \vec{E} \cdot d\vec{l} = \frac{d\Phi_B}{dt}. \quad (1.8)$$

Therefore, magnetic field has to be computed.

Following are the assumptions about the magnetic field distribution:

- Magnetic field flows only between and within the ferromagnetic plates, and does not exit the generator;
- Magnetic field lines are perpendicular to the surfaces of the plates between the plates;
- Magnetic field is homogeneous in every medium, be it magnet, air or gadolinium;⁵
- Magnetic field flows "up" in permanent magnet and "down" in air and gadolinium;
- Permanent magnet is the dominant source of magnetic field in the generator.

These assumptions are justified, when distance between plates h is much smaller than the other dimensions of the plates. The justification is similar to that for distribution of electric field between two charged conductive plates (as in plate capacitor); in this case magnetic field replaces electric field [19].

Magnetic field distribution is shown in figure 3.

To calculate concrete values of magnetic induction B , Ampère's circuital theorem⁶ can be

⁵Relative magnetic permeability of ferromagnetic plates $\mu_r \gg 1$, so that every point of the plate has similar magnetic potential.

⁶Operating under assumption, that no free electric currents flow through the contour.

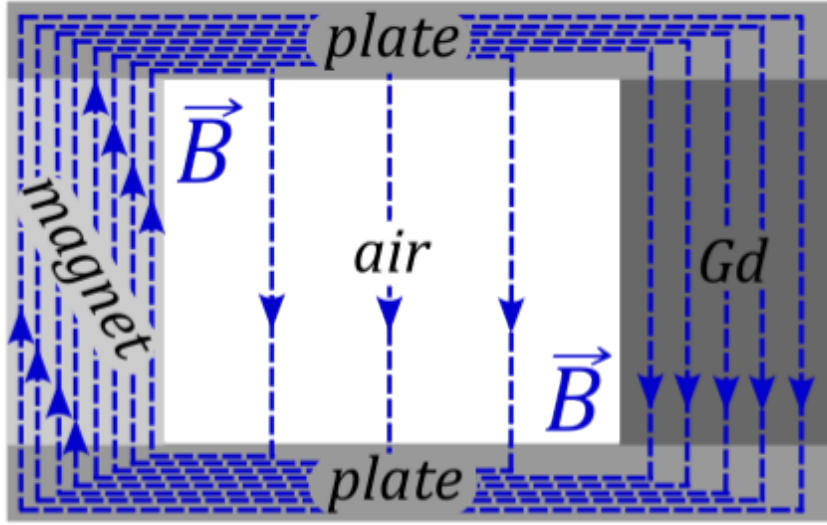


Figure 3. Magnetic field distribution in the generator in case of a single gadolinium bar configuration

used:

$$\oint_L \vec{H} \cdot d\vec{l} = 0, \quad (1.9)$$

where \vec{H} is magnetic field strength.

For the first configuration (see figure 1), two rectangular contours are used (see figure 4): contour through gadolinium and air, and contour through magnet and air. In horizontal components of the contours dot product $\vec{H} \cdot d\vec{l} = 0$; in vertical components of the contours, dot product $\vec{H} \cdot d\vec{l} = H dl$.

From electromagnetism [19] it is known that:

$$\vec{H} = \frac{\vec{B}}{\mu_0} - \vec{M}. \quad (1.10)$$

According to assumptions stated above, in every medium $\vec{H} \parallel \vec{B} \parallel \vec{M}$, therefore:

$$H = \frac{B}{\mu_0} - M. \quad (1.11)$$

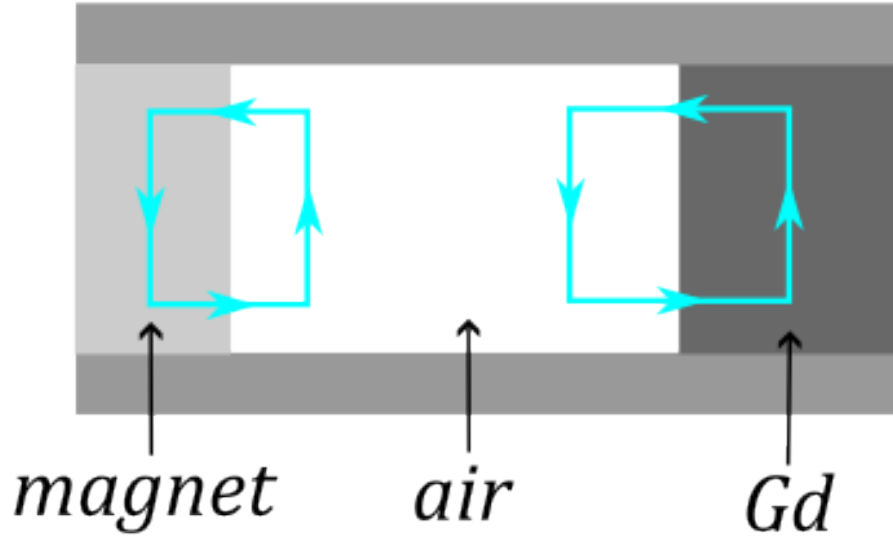


Figure 4. Ampère's circuital theorem in case of a single gadolinium bar configuration

Thus, for every medium:

$$\begin{aligned}
 H_{\text{Gd}} &= \frac{B_{\text{Gd}}}{\mu_0} - M_{\text{Gd}}, \\
 H_{\text{magnet}} &= \frac{B_{\text{magnet}}}{\mu_0} - M_{\text{magnet}}, \\
 H_{\text{air}} &= \frac{B_{\text{air}}}{\mu_0}.
 \end{aligned} \tag{1.12}$$

Since the contours are rectangular, vertical sides have the same length, and this length can be reduced immediately, both sides can be multiplied by μ_0 . When adding to the two equations from Ampère's circuital theorem continuity condition: magnetic flux "down" is equal to magnetic flux "up", or

$$\oint_A \vec{B} \cdot d\vec{A} = 0, \tag{1.13}$$

where A is a plane that cuts through the middle section of the generator perpendicularly to the magnetic field and is closed through the infinity point, the following system of linear equations is acquired:

$$\begin{cases}
 -B_{\text{magnet}} + \mu_0 M_{\text{magnet}} - B_{\text{air}} = 0, \\
 B_{\text{air}} - B_{\text{Gd}} + \mu_0 M_{\text{Gd}} = 0, \\
 B_{\text{Gd}} A_{\text{Gd}} + B_{\text{air}} A_{\text{air}} - B_{\text{magnet}} A_{\text{magnet}} = 0.
 \end{cases} \tag{1.14}$$

Here, areas A_{Gd} , A_{air} and A_{magnet} are known, gadolinium magnetization M_{Gd} is taken from equation 1.2, permanent magnet magnetization is assumed to be constant:

$$M_{\text{magnet}} = \frac{B_r}{\mu_0}, \quad (1.15)$$

where B_r is permanent magnet remanence. Thus, this is a system of three equations with three unknowns. Gadolinium magnetic induction in case of a **single gadolinium bar** configuration can be expressed:

$$B_{\text{Gd}} = \frac{B_r A_{\text{magnet}} + \mu_0 M_{\text{Gd}} (A_{\text{air}} + A_{\text{magnet}})}{A_{\text{Gd}} + A_{\text{air}} + A_{\text{magnet}}}. \quad (1.16)$$

For the second configuration (see figure 2), a third contour is added through the second gadolinium bar and air, entirely analogous to how it was done before. This yields the following system for the **double gadolinium bar** configuration:

$$\begin{cases} -B_{\text{magnet}} + \mu_0 M_{\text{magnet}} - B_{\text{air}} = 0, \\ B_{\text{air}} - B_{\text{Gd}_1} + \mu_0 M_{\text{Gd}_1} = 0, \\ B_{\text{air}} - B_{\text{Gd}_2} + \mu_0 M_{\text{Gd}_2} = 0, \\ B_{\text{Gd}_1} A_{\text{Gd}_1} + B_{\text{Gd}_2} A_{\text{Gd}_2} + B_{\text{air}} A_{\text{air}} - B_{\text{magnet}} A_{\text{magnet}} = 0. \end{cases} \quad (1.17)$$

Then, magnetic fields:

$$\begin{cases} B_{\text{Gd}_1} = \frac{B_r A_{\text{magnet}} + \mu_0 M_{\text{Gd}_1} (A_{\text{Gd}_2} + A_{\text{air}} + A_{\text{magnet}}) - \mu_0 (M_{\text{Gd}_2} A_{\text{Gd}_2})}{A_{\text{Gd}_1} + A_{\text{Gd}_2} + A_{\text{air}} + A_{\text{magnet}}}, \\ B_{\text{Gd}_2} = B_{\text{Gd}_1} - \mu_0 M_{\text{Gd}_1} + \mu_0 M_{\text{Gd}_2}. \end{cases} \quad (1.18)$$

Similarly, magnetic field can be calculated in **triple gadolinium bar** case:

$$\begin{cases} -B_{\text{magnet}} + \mu_0 M_{\text{magnet}} - B_{\text{air}} = 0, \\ B_{\text{air}} - B_{\text{Gd}_1} + \mu_0 M_{\text{Gd}_1} = 0, \\ B_{\text{air}} - B_{\text{Gd}_2} + \mu_0 M_{\text{Gd}_2} = 0, \\ B_{\text{air}} - B_{\text{Gd}_3} + \mu_0 M_{\text{Gd}_3} = 0, \\ B_{\text{Gd}_1} A_{\text{Gd}_1} + B_{\text{Gd}_2} A_{\text{Gd}_2} + B_{\text{Gd}_3} A_{\text{Gd}_3} + B_{\text{air}} A_{\text{air}} - B_{\text{magnet}} A_{\text{magnet}} = 0. \end{cases} \quad (1.19)$$

Then:

$$\begin{cases} B_{\text{Gd}_1} = \frac{B_r A_{\text{magnet}} + \mu_0 M_{\text{Gd}_1} (A_{\text{Gd}_2} + A_{\text{Gd}_3} + A_{\text{air}} + A_{\text{magnet}}) - \mu_0 (M_{\text{Gd}_2} A_{\text{Gd}_2} + M_{\text{Gd}_3} A_{\text{Gd}_3})}{A_{\text{Gd}_1} + A_{\text{Gd}_2} + A_{\text{Gd}_3} + A_{\text{air}} + A_{\text{magnet}}}, \\ B_{\text{Gd}_2} = B_{\text{Gd}_1} - \mu_0 M_{\text{Gd}_1} + \mu_0 M_{\text{Gd}_2}, \\ B_{\text{Gd}_3} = B_{\text{Gd}_1} - \mu_0 M_{\text{Gd}_1} + \mu_0 M_{\text{Gd}_3}. \end{cases} \quad (1.20)$$

Additionally, magnetic field is affected by generated current, however the effect is much smaller. The generator coil produces by far the strongest magnetic field among electric components of a generator, so it should be accounted for first. From electromagnetism [19], it is known that self-inductance L of a solenoid can be calculated according to following equation with number of loops N , length l and cross section area A :

$$L = \frac{\mu_r \mu_0 N^2 A}{l}. \quad (1.21)$$

In linear magnetization case $H = \frac{B}{\mu_r \mu_0}$. Gadolinium magnetization might not be linear, so equation 1.11 should be used. Since the effect of inductances is small compared to that of permanent magnet, the connection between magnetic induction B and magnetic field strength H can be assumed to be locally linear for approximation purposes:⁷

$$\begin{aligned} \mu_r \mu_0 &= \frac{B_{\text{Gd}}}{H_{\text{Gd}}} = \frac{B_{\text{Gd}}}{\frac{B_{\text{Gd}}}{\mu_0} - M_{\text{Gd}}} = \frac{\mu_0}{1 - \mu_0 \frac{M_{\text{Gd}}}{B_{\text{Gd}}}}, \\ L &= \frac{\mu_0 N^2 A}{\left(1 - \mu_0 \frac{M_{\text{Gd}}}{B_{\text{Gd}}}\right) l}. \end{aligned} \quad (1.22)$$

This self-inductance can be used in further calculations.

From definition, $L = \frac{\Phi_{B_{\text{coil}}}}{I}$, where $\Phi_{B_{\text{coil}}}$ is magnetic flux caused by coil self-inductance, so magnetic field inside coil with current:

$$B_{\text{self}} = \frac{\mu_0 N^2 I}{\left(1 - \mu_0 \frac{M_{\text{Gd}}}{B_{\text{Gd}}}\right) l}. \quad (1.23)$$

For double and triple coil generator configuration, mutual inductance magnetic field B_{mut} has to be calculated for every coil pair. One possible approach is to calculate mutual inductance M_L . It is known from electromagnetism [19], that $M_L = \frac{\Phi_{B_{\text{coil}}}}{I}$, where $\Phi_{B_{\text{coil}}}$ is magnetic field flux caused by one coil in the other coil. Due to assumptions,

$$M_L = \frac{B_{\text{mut}} A}{I} \Rightarrow B_{\text{mut}} = \frac{M_L I}{A}. \quad (1.24)$$

The second approach is more feasible in the context of this thesis. Due to superposition principle, the magnetic field caused by different sources can be looked at separately. In case of magnetic field from electric current in one coil in place of another coil, we can apply Ampère's circuital theorem with free currents for a contour, that passes through two gadolinium bars

⁷It should be noted, that this approximation is questionable, and must be revised if a more precise modelling is to be made, and in case of larger electric currents.

parallel to the magnetic field, and is otherwise perpendicular to the magnetic field:

$$\oint H dl = \sum_i I_i = NI, \quad (1.25)$$

where N is number of source coil loops, and I is current in the source coil.

Using equation 1.22 and again assuming locally linear behaviour of magnetization:

$$\begin{aligned} \frac{B_{\text{receiver}}}{\mu_{\text{r,receiver}}\mu_0} + \frac{B_{\text{source}}}{\mu_{\text{r,source}}\mu_0} &= nI, \\ B_{\text{receiver}} &= \mu_{\text{r,receiver}}\mu_0 nI - \frac{\mu_{\text{r,receiver}}\mu_0 B_{\text{source}}}{\mu_{\text{r,source}}\mu_0}, \end{aligned} \quad (1.26)$$

where $n \equiv \frac{N}{l}$ is coil loop density, $\mu_{\text{r,receiver}}$ is receiver relative permeability, $\mu_{\text{r,source}}$ is source relative permeability, and B_{source} is calculated self-inductance field in the source coil (see equation 1.23).

When mutual inductance fields from all coils are calculated, they can be combined with field caused by the permanent magnet, according to superposition principle, getting

$$B_{\mathcal{E}} = B_{\text{magnet}} + \sum_i B_{i,\text{receiver}}, \quad (1.27)$$

the change of which can be used to calculate electromotive force in the output coil, self-inductance is accounted for later in the calculations. Total magnetic field

$$B_{\text{total}} = B_{\text{magnet}} + B_{\text{self}} + \sum_i B_{i,\text{receiver}} \quad (1.28)$$

can be used to calculate gadolinium properties.

1.5 Electricity Generation

Electromotive force can be found from equation 1.8, here $\Phi_B \equiv \vec{B} \cdot \vec{A}$ is magnetic field \vec{B} flux through area \vec{A} . According to assumptions $\vec{B} \parallel \vec{A}$, therefore:

$$\Phi_B = BA. \quad (1.29)$$

If a coil is placed around gadolinium bars⁸, $B = B_{\text{Gd}}$, $A = A_{\text{Gd}}N$, where N is number of coil loops.

⁸This seems to be a reasonable location: gadolinium magnetization changes cause electricity generation; the coil can be used as a part of heat exchanger; gadolinium bar height, cross section area and magnetic field are already used in the calculations.

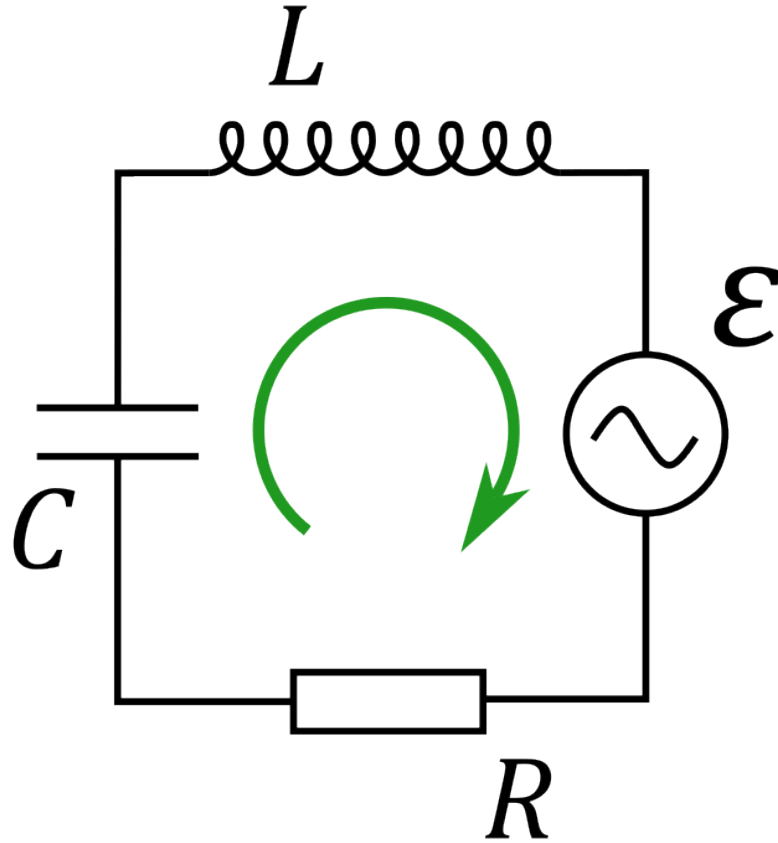


Figure 5. Simplified circuit connected to a single generator coil⁹

The time derivative of magnetic flux $\frac{d\Phi_B}{dt}$ can be approximated as $\frac{\Delta\Phi_B}{\Delta t}$, where $\Delta\Phi_B$ is small (but not infinitesimal) change in magnetic field flux Φ_B during small (but not infinitesimal) time period Δt .

Generator coil has self-inductance, as shown in equation 1.22. This inductance introduces phase shift in case of an alternating current (which is expected as a result of oscillating temperature) into the circuit, which reduces output power. A capacitor connected in series can be introduced to compensate for this shift. The circuit has ohmic resistance $R = R_{\text{coil}} + R_{\text{load}}$, inductance L , capacitance C and electromotive force \mathcal{E} (see figure 5). Using Kirchhoff's second law [19] a differential equation can be constructed:¹⁰

$$L\ddot{q} + R\dot{q} + \frac{1}{C}q + \mathcal{E} = 0. \quad (1.30)$$

Because $L(B, T)$, the equation becomes overly complex, therefore it is appropriate to use numerical methods to find the solution.

⁹Here, a symbol for alternating current is used to represent electromotive force; the current is, in fact, not guaranteed to be sinusoidal.

¹⁰Here, $\dot{x} \equiv \frac{dx}{dt}$ and $\ddot{x} \equiv \frac{d^2x}{dt^2}$, so $\dot{q} = I$.

In case of multiple coils, mutual inductance is accounted for in calculation of electromotive force \mathcal{E} , so no changes are needed in case of more complicated configurations.

For every coil in the generator this equation has to be solved. This can be done numerically.

Then, total voltage in the circuit $U \equiv \mathcal{E}$ and current I are found. Effective voltage over period t can be calculated as follows:

$$U_{\text{eff}} = \frac{1}{t} \sqrt{\int_0^t U^2 dt}, \quad (1.31)$$

and effective power over period t can be found as:

$$P = \frac{1}{t} \int_0^t UI dt. \quad (1.32)$$

Power output over any small enough period of time dt (so that voltage and current can be assumed to be locally constant) is then:

$$P = UI. \quad (1.33)$$

Here, negative power would represent power used by the generator to cause gadolinium temperature change in normally thermodynamically impossible direction with magnetocaloric effect.

These calculations, again, should be done for every coil separately.

2. Data Preparation

This chapter describes data acquisition and processing required to simulate the generator. Extracted data is presented in appendix 2.

2.1 Acquisition

The data has been provided in form of graphs [6]. To make this data usable, it has to be digitized. For this purpose, an online tool was used [28].

The original research includes:

- Gadolinium magnetization against magnetic induction at multiple temperatures;
- Gadolinium magnetization against temperature at multiple magnetic induction values;
- Gadolinium magnetic susceptibility against temperature;
- Gadolinium heat capacitance against temperature at multiple magnetic induction values;
- Gadolinium temperature change due to magnetocaloric effect in known pulsed magnetic field against temperature.

These data types were chosen:

- Gadolinium magnetization against magnetic induction along 0001 crystal lattice axis of gadolinium at temperatures 237.0 K, 247.2 K, 267.6 K, 277.8 K, 288.1 K, 298.4 K, 318.9 K and 324.0 K;
- Gadolinium magnetization against magnetic induction along 1010 crystal lattice axis of gadolinium at temperatures 236.9 K, 247.1 K, 267.6 K, 277.4 K, 288.0 K, 298.4 K, 318.8 K and 324.0 K;
- Gadolinium heat capacitance against temperature at magnetic induction values 0.0 T, 2.0 T, 5.0 T, 7.5 T and 10.0 T;
- Gadolinium calculated magnetocaloric effect against temperature in pulsed magnetic field (for validation purposes) $B : 0.0 \text{ T} \rightarrow 2.0 \text{ T}$.

2.2 Interpolation

Since acquired data is only defined for a few points, interpolation is required. Data on gadolinium heat capacitance and magnetization is three-dimensional, while magnetocaloric effect data is two-dimensional; thus, appropriate interpolation methods are to be used.

In both cases, *Python* module *SciPy* was used for interpolation [24]. For three-dimensional data types smooth bivariate cubic spline was used; for two two-dimensional data single

variable cubic spline was used. No extrapolation is required.

The processed data can be used as functions:

- Gadolinium heat capacitance c_ν is a function of magnetic induction B and temperature T (so, $c_\nu(B, T)$); this function returns heat capacitance in $\frac{\text{J}}{\text{mol}\cdot\text{K}}$, which is converted to $\frac{\text{J}}{\text{m}^3\cdot\text{K}}$ (see equation 1.3); the function is defined for $B \leq 10$ T and $T \leq 350$ K;
- Both directions of gadolinium magnetization M_{0001} and M_{1010} are functions of magnetic induction B and temperature T (so, $M_{0001}(B, T)$ and $M_{1010}(B, T)$); these functions return magnetization in $\frac{\text{m}^2\cdot\text{A}}{\text{kg}}$, which is converted to $\frac{\text{A}}{\text{m}}$ (see equation 1.2); additionally, an average of two magnetizations is taken; the functions are defined for $B \leq 5.6$ T and 237 K $\leq T \leq 324$ K;
- Temperature change due to magnetocaloric effect ΔT is a function of temperature T (so, $\Delta T(T)$); this function returns magnetocaloric effect in K; the function is defined for 100 K $\leq T \leq 330$ K.

2.3 Validation

All plotting is done with *Matplotlib* [25].

Figure 6 contains interpolated three-dimensional data slices at selected values of temperature T or magnetic induction B : gadolinium magnetization (top-left is 0001-axis magnetization, bottom-left is 1010-axis magnetization), and gadolinium heat capacitance (top-right).

The resulting curves are similar to those in the original research. Spike in the heat capacitance graph at $T \approx 290$ K, $B = 0$ T and the smoothing of the curve at stronger magnetic fields are expected from data presented in the research. The behavior of the magnetization graphs agrees with that presented in the research. The numerical data (after unit conversion) is also similar. [6]

For additional validation, magnetocaloric effect can be calculated from heat capacitance and compared to the calculations of the original research [6]. For this, new temperature after magnetic field change T_1 has to be found. Equation 1.5 can be rewritten for molar heat capacitance at known magnetic induction B_0 :

$$dQ = c_{\nu, B_0} \nu dT. \quad (2.1)$$

From integrating both parts:

$$Q = \int_0^{T_0} c_{\nu, B_0} \nu dT, \quad (2.2)$$

which is total heat stored in ν moles of gadolinium at temperature T_0 and magnetic field B_0 . If magnetic field changes to a new value B_1 (new temperature is T_1), the heat stored in

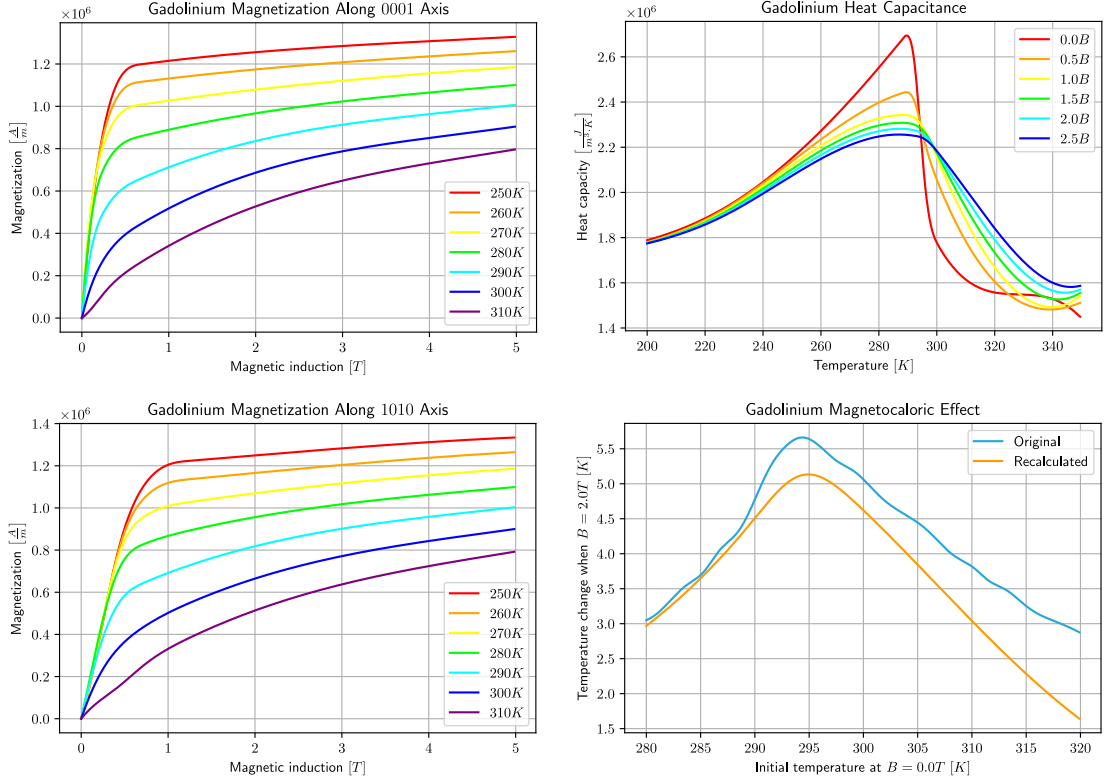


Figure 6. Interpolated data visualization and validation

gadolinium should not change due to law of conservation of energy, so¹

$$\int_0^{T_1} c_{\nu, B_1}(T) dT = \int_0^{T_0} c_{\nu, B_0}(T) dT. \quad (2.3)$$

Assuming that the indefinite analogues of the above integrals yield corresponding antiderivatives ρ_{B_1} and ρ_{B_0} which represent molar heat energy density, equation 2.3 can be rewritten as

$$\rho_{B_1}(T_1) - \rho_{B_1}(0) = \rho_{B_0}(T_0) - \rho_{B_0}(0). \quad (2.4)$$

If $\rho_{B_1}(0) = \rho_{B_0}(0) = 0$, which can be assumed since heat energy density of gadolinium is the same at temperature $T = 0$ at every magnetic induction B value, equation 2.4 transforms:²

$$\rho_{B_1}(T_1) - \rho_{B_0}(T_0) = 0. \quad (2.5)$$

In this equation, $\rho_{B_0}(T)$ and $\rho_{B_1}(T)$ can be calculated using numerical integration from known temperature T . Since $\frac{d\rho_{B_1}(T_1)}{dT_1} = c_{\nu, B_1}(T)$, and $\rho_{B_0}(T_0)$ is a constant so $\frac{d\rho_{B_0}(T_0)}{dT_1} = 0$, the equation 2.5 can be solved for T_1 using Newton's iteration method,³ where T_{i-1} is temperature

¹Since ν is a constant, it can be disregarded.

²The physical meaning of this equation is that heat energy density must not change due to magnetocaloric effect.

³Newton's iteration method is applicable for equations in form $f(x) = 0$, and every next iteration approaches the solution of the equation: $x_i = x_{i-1} - \frac{f(x_{i-1})}{f'(x_{i-1})}$.

in the previous iteration, and T_i is temperature in the current iteration:

$$T_i = T_{i-1} - \frac{\rho_{B_1}(T_{i-1}) - \rho_{B_0}(T_0)}{c_{\nu, B_1}(T_{i-1})}. \quad (2.6)$$

The calculations are stopped when precision condition is fulfilled, in this case the condition is: $\eta \equiv |T_i - T_{i-1}| < 1 \times 10^{-6}$ K. Thus, T_1 has been calculated. Magnetocaloric effect is $\Delta T = T_1 - T_0$. The resulting values are plotted with the calculations from the original research [6] in figure 6 (bottom-right).

The graphs are similar and follow the same pattern: within 0.5 K deviation. The discrepancies seem to come from interpolation artifacts at the earlier mentioned spike in heat capacitance graph at $B = 0$ T and $T \approx 290$ K. Since the integration starts from $T = 0$ K, the error accumulates. At stronger magnetic field, it is reasonable to expect, that error will decrease due to heat capacitance curve getting smoother.

3. Generator Simulation

This chapter presents methods used in the simulation. Most processes are calculated in separate functions, which are later put together and applied during the simulation. Simulation code is presented in appendix 2.

3.1 Magnetic Field Distribution

To calculate magnetic field, magnetization of gadolinium M_{Gd} is required. It can be directly found from earlier interpolated data (see chapter 2). An average of both magnetizations is taken to account for random orientation of gadolinium crystal lattice in the bars.

Additionally, a function symmetry condition is to be added. Magnetization interpolant $M_{Gd,int}(B, T)$ is only defined for positive magnetic induction B , so in order to account for negative magnetic induction (which is simply pointed the opposite direction), a new function can be defined:¹

$$M_{Gd} = \begin{cases} M_{Gd,int}(B, T), & B > 0, \\ -M_{Gd,int}(-B, T), & B < 0, \\ 0, & B = 0. \end{cases} \quad (3.1)$$

Magnetic field in a single gadolinium bar B_{Gd} depends on temperature of every gadolinium bar, current in every generator coil, and every gadolinium bar magnetization. Thus, all magnetic fields should be calculated within a single function. Equations 1.16, 1.18 and 1.20 can be used for magnet-originating magnetic field calculations; equation 1.23 can be used to calculate self-inductance magnetic field; equation 1.26 can be used to calculate mutual inductance magnetic field.

The calculated fields can be added together due to superposition principle. If sign rule is defined and followed, no additional work is to be done. In gadolinium bar, "downward" magnetic induction as shown in figure 3 is defined as positive.

Two types of magnetic fields are defined: total magnetic induction $B_{total} = B_{magnet} + B_{self} + \sum_i B_{i,mutual}$ is used for gadolinium heat capacitance; and electromotive magnetic induction $B_{\mathcal{E}} = B_{magnet} + \sum_i B_{i,mutual}$ is used for electromotive force calculation. Additionally, only permanent magnet magnetic field B_{magnet} is used to calculate the magnetization, this is possible due to an assumption that permanent magnet magnetic field is dominant. Effects of self-inductance magnetic field on the electrical circuit are calculated using self-inductance L .

¹Since gadolinium is a soft ferromagnetic material, $M_{Gd}(B = 0) = 0$.

3.2 Thermodynamic Processes

For temperature change in gadolinium caused by magnetocaloric effect, similar methods to those in chapter 2 are used. Heat stored in a gadolinium Q at temperature T can be calculated as integral of heat capacitance C over temperature:

$$Q = \int_0^T C dT = V \int_0^T c_V dT. \quad (3.2)$$

Since gadolinium volume heat capacitance interpolant is acquired and volume is assumed to be constant, numerical integration methods can be used.

To calculate gadolinium temperature from stored heat, an integral equation has to be solved. Since amount of heat does not change with changing magnetic induction B due to law of conservation of energy:

$$V \int_0^{T_1} c_{V,B_1}(T) dT = V \int_0^{T_0} c_{V,B_0}(T) dT, \quad (3.3)$$

where T_1 is new temperature, B_1 is new magnetic induction, T_0 is initial temperature, and B_0 is initial magnetic induction. Let

$$f_B(T) = c_{V,B}(T) \quad (3.4)$$

and

$$F_B(T) \equiv \rho_B(T) = \int c_{V,B}(T) dT, \quad (3.5)$$

where B is some constant magnetic induction. Analogous to the method shown in the end of chapter 2, equation 3.3 can be solved using Newton's iteration method for T_1 :

$$T_i = T_{B_0} - \frac{F_{B_1}(T_{i-1}) - F_{B_0}(T_0)}{f_{B_0}(T_{i-1})}, \quad (3.6)$$

where T_{i-1} is temperature in the previous iteration, and T_i is temperature in the current iteration; $i \rightarrow \infty \Rightarrow T_1 = T_i$.

Additionally, outside heat ΔQ is introduced to the system.² Using heat flux $W = K\Delta T$, where K is heat transfer parameter and ΔT is temperature difference, and time step of the simulation Δt , introduced heat $\Delta Q = W\Delta t$. This heat is distributed equally (by volume) in the gadolinium bar so that temperature stay homogeneous.

Using introduced heat equations and magnetocaloric effect in conjunction with magnetic induction function, gadolinium temperature change can be calculated at a new point of time

²Introduction of negative heat is possible in this case as well.

$t_1 = t_0 + \Delta t$. To achieve this, total heat stored in gadolinium at $t = t_1$ is calculated:

$$Q_1 = Q_0 + W\Delta t, \quad (3.7)$$

where Q_0 is heat stored in gadolinium at $t = t_0$, W is heat flux from the heat exchanger, and $\Delta t = t_1 - t_0$. From new heat Q_1 new temperature T_1 can be calculated using Newton's iteration method 3.6 with $\eta \equiv |T_i - T_{i-1}| < 1 \times 10^{-6}$ K as a precision condition.

3.3 Electricity Generation

Electromotive force can be calculated from equation 1.8, where $\Phi_B = \vec{B} \cdot \vec{A}$ is magnetic flux through area A . In this case, $A = A_{\text{Gd}}$, and $\vec{B} \parallel \vec{A}$. Additionally, area A_{Gd} should be multiplied by number of coil loops N_{coil} to account for magnetic flux passing through multiple cross sections. Then, negative numerical time derivative of magnetic flux can be expressed as:

$$\mathcal{E} \equiv -\frac{d\Phi_B}{dt} \approx -\frac{(B_1 - B_0)N_{\text{coil}}A_{\text{Gd}}}{\Delta t}, \quad (3.8)$$

where B_0 and B_1 are respectively magnetic inductions at start and end of time period Δt .

Next, whole circuit state has to be calculated. For this, equation 1.30 can be used, so a sign rule has to be defined. In a case where L , R , C and \mathcal{E} are all constant (stationary case), we can take a look at initial state (circuit has just been closed) and final state (a long time has passed since the circuit has been closed).

Firstly, resistance R is always directed against electromotive force \mathcal{E} , so their signs have to be opposite. Next, just after the circuit has been closed, capacitor charge $q = 0$, and self-inductance L works against electromotive force \mathcal{E} , so their signs have to be opposite. Finally, after the capacitor has accumulated sufficient charge q no current flows through the circuit, so \mathcal{E} is compensated entirely by capacitance C , therefore their signs must be opposite.

Then, the following equation is arrived at:

$$-L\ddot{q} - R\dot{q} - \frac{1}{C}q + \mathcal{E} = 0. \quad (3.9)$$

Assuming some initial current I_0 and initial capacitor charge q_0 , current time derivative $\frac{dI}{dt} \equiv \ddot{q}$ can be found:

$$\frac{dI}{dt} \approx \frac{\mathcal{E} - RI_0 - \frac{q_0}{C}}{L}. \quad (3.10)$$

Using current time derivative, it is possible to find new current I after some small time Δt :

$$I \approx I_0 + \frac{dI}{dt}\Delta t. \quad (3.11)$$

And using an average of these two currents, new capacitor charge q after time Δt can be found:

$$q \approx q_0 + \frac{I_0 + I}{2} \Delta t. \quad (3.12)$$

Thus, there is a method to find new circuit state from initial one after some small period of time.³

Although this method is good enough for a single gadolinium bar generator, in other cases the convergence is uncertain and slow. Therefore, *SciPy* library integration module will be used for the solution of this equation instead of the above method [24].

Second order differential equation has to be transformed into a system of first order differential equations since only first order equations are solved by the ordinary differential equation integration function [24]:

$$\begin{cases} \frac{dq}{dt} = I, \\ \frac{dI}{dt} = \frac{\mathcal{E} - RI - \frac{q}{C}}{L}. \end{cases} \quad (3.13)$$

By setting some starting conditions $I(t_0) = I_0$, $q(t_0) = q_0$, electric current and charge at the next time frame $t_0 + \Delta t$ can be calculated.

Power output at any moment of time from the generator can be calculated from equation 1.33.⁴ This is the total power output on every resistive part of the generator. To account for non-zero resistance of the coil, ratio of resistances has to be added:

$$P_{\text{out}} = \frac{R_{\text{load}}}{R_{\text{load}} + R_{\text{coil}}} UI. \quad (3.14)$$

Additionally, averaged voltage and power can be calculated. Output voltage⁵ can be calculated as root mean square of electromotive force adjusted by resistance ratio:

$$U_{\text{trms}} = \frac{R_{\text{load}}}{R_{\text{load}} + R_{\text{coil}}} \sqrt{\frac{1}{n} \sum_{i=1}^n U_i^2}. \quad (3.15)$$

Output power can be calculated as a simple mean of earlier calculated power outputs during some small periods of time (see equation 3.14):

$$P_{\text{mean}} = \frac{1}{n} \sum_{i=1}^n P_i. \quad (3.16)$$

³This time period Δt has to be small enough, so that L , R , C and \mathcal{E} can be assumed to be constant during this time period; otherwise, this solution may not converge.

⁴In fact, electromotive force is used here instead of voltage.

⁵Note that this would be output voltage only if the circuit is open, and even then there are some minor differences; this value can be used for comparison and demonstration, otherwise output power is a better parameter.

3.4 Simulation

The differential equations that describe the generator can be solved using the Euler method (see chapter 1).

The simulation calculates generator state during a defined simulation time t with time step Δt . New generator state is calculated based on state in the previous time frame. Thus, by setting some initial conditions (the most straightforward solution is setting temperature to an average of hot and cold liquid temperature, every other parameter is set to zero), generator state can be calculated during the whole time of the simulation. During one time frame, most parameters are assumed to be constant or linear, so a small enough Δt is required for this solution to converge.

Equations derived above are used as functions in the simulation.

Firstly, magnetic field distribution in the generator is calculated; this includes both total and electromotive magnetic fields in every gadolinium bar, as well as magnetic fields caused by permanent magnet.

Secondly, every gadolinium bar temperature is calculated; this is the most computationally intensive part of the simulation due to multiple numerical methods being used.

Thirdly, electromotive force on every generator coil is calculated from magnetic field change between previous and current time frames.

Finally, differential equation for circuit state is solved and new electric current, capacitor charge and power output are calculated. The circuit state calculations only begin after one second has passed in the simulation to ensure that the generator has reached equilibrium before magnetic field from electric current is introduced.

The circuit state differential equation 3.9 is the biggest factor in convergence uncertainty, so its solution results have to be used to determine appropriate time step Δt .

The best use case for the model is to compare different conditions. For this purpose, a series option is introduced: it allows to run multiple simulation in series with varying parameters. Thus, a set of test parameters is used, and output data is automatically collected from every simulation to be compared later. These output data values are calculated based on the last oscillation of the generator during the time t to ensure that the generator had enough time to reach equilibrium state.

Simulation is expected to be a computationally intensive process, so visual progress representation is recommended. During series simulation, completed and total number of simulations is shown. Additionally, progress of every separate simulation is shown in percents.

3.5 Visualization of Results

For the purpose of visualization of the results, three options are available; *Matplotlib* library is used [25].

Single oscillation graphs show every gadolinium bar parameters during one final simulated oscillation. The plotted parameters are:

- Gadolinium bar temperature in kelvins with a line representing gadolinium Curie temperature;
- Total magnetic induction in a gadolinium bar in teslas;
- Electromotive force produced by the coil in volts;
- Electric current flowing through the circuit in amperes;
- Capacitor charge in coulombs;
- Generator load power output in watts.

In case of multiple gadolinium bars, the graphs are plotted in the same axes, and different bars are plotted with different colours.

Similarly, long-term graphs can be plotted with the stated above gadolinium parameters. These graphs show long-term tendencies of the parameters; all data after one second in the simulation is plotted. This is most helpful in observing capacitor charge convergence to some stable oscillation pattern. Again, different gadolinium bars are plotted with different colours.

The third option is series graphs plotting. Here, maximum and minimum temperatures are plotted and generator temperature range is visualized, Curie temperature line is provided for reference. Next, effective voltage on the generator load is plotted. And finally, effective power output on the generator load is plotted. This time, data from only one gadolinium bar is used, as they are expected to be identical in terms of mean values. Only last oscillation is used in the calculations. *X*-axis of series graphs has to be manually set, as there is no easy way to define the axis for every possible combination of changing generator parameters.

4. Results

In this chapter, the results of the modelling are presented and analyzed.

4.1 Triple Gadolinium Bar Simulation Results

As mentioned before, the calculations are computationally intensive and might take a long time to complete. The time is proportional to number of gadolinium bars N_{Gd} and simulation time t , and inversely proportional to time step Δt . Other parameters do not seem to have any noticeable effect on the time it takes to complete the simulation.

Number of gadolinium bars N_{Gd} describes generator configuration. While it is important to account for multiple bars in some cases, in most cases it is reasonable to simulate single bar generator to reduce simulation time.

Simulation time t is required to be longer than one second to allow the generator to reach stable equilibrium state from arbitrary starting conditions. Then, at least one full oscillation has to be completed for the purposes of data collection; however, additional oscillations allow for better accuracy. Additionally, longer simulation time can be used to observe slower processes, such as capacitor charge convergence to stable oscillation pattern from chaotic behaviour that may be present in the beginning of the simulation.

Time step Δt is directly tied to simulation convergence. It is obvious, that Δt has to be much smaller than the time it takes to complete one oscillation (so $\Delta t \ll \frac{1}{f}$). Additionally, equation 3.9 solution may not converge at too high Δt values.

In case of derived simple solution of equation 3.9, it has been found experimentally, that time step $\Delta t = 1 \times 10^{-3}$ s ensures convergence in case of a single gadolinium bar, for more gadolinium bars $\Delta t = 1 \times 10^{-4}$ s is required. Time step $\Delta t \leq 1 \times 10^{-5}$ s can be used, but seems to give only marginal improvement over the previous cases, while requiring much more time to complete the simulation.

In case if *SciPy* integration module is used for the solution of equation 3.9, convergence can be achieved at $\Delta t = 1 \times 10^{-2}$ s in every case, however $\Delta t = 1 \times 10^{-3}$ s or $\Delta t = 1 \times 10^{-4}$ s are preferred due to higher accuracy. Again, $\Delta t \leq 1 \times 10^{-5}$ s will only yield marginal improvements.

Next, results for some arbitrary starting conditions are provided for demonstration purposes. For all graphs in the remaining part of this section, distance between generator plates $h = 1$ cm, ferromagnetic plate air contact surface area $A_{\text{air}} = 16$ cm², heat transfer parameter between

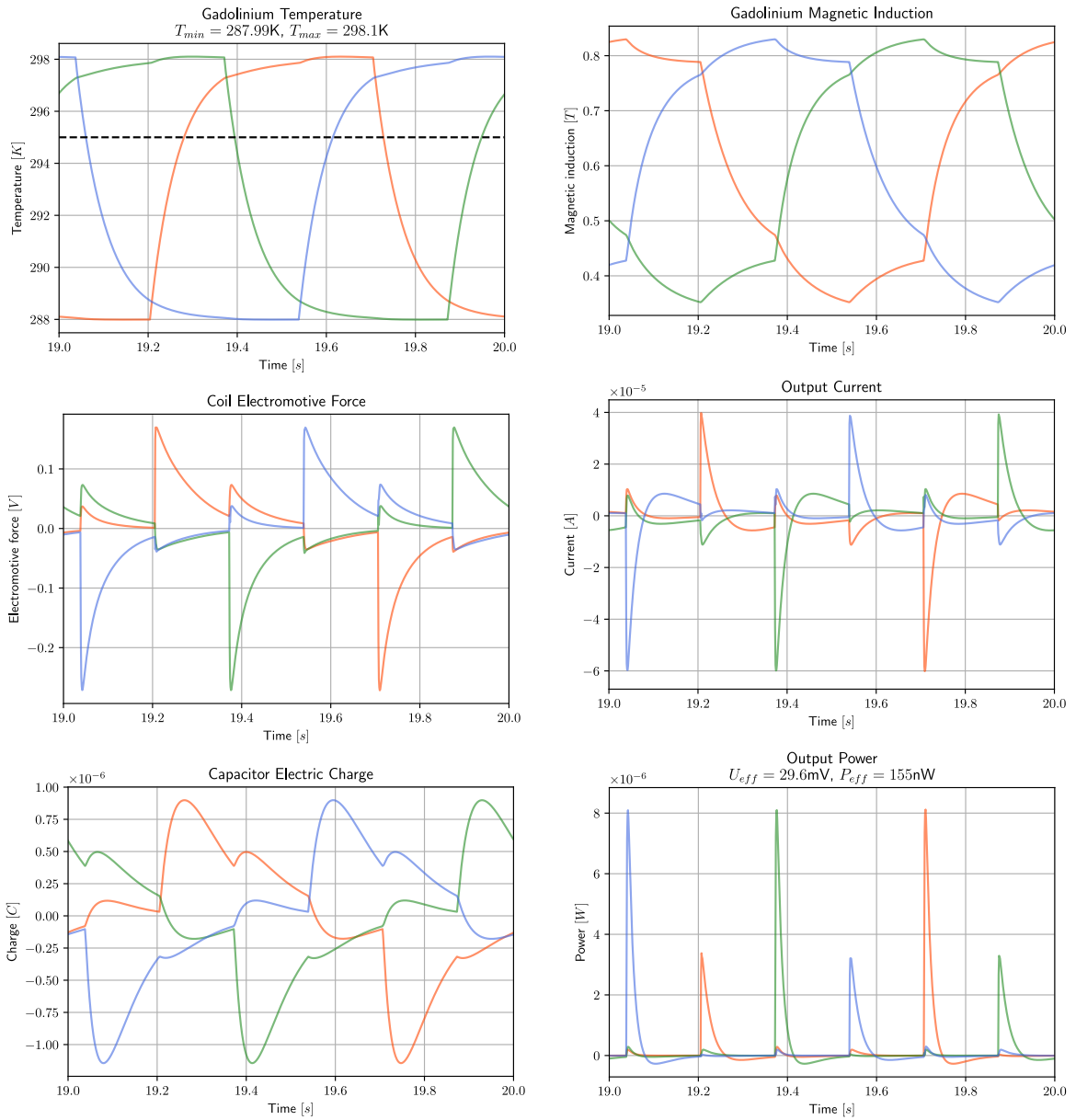


Figure 7. Final oscillation time graphs of (left to right, top to bottom) temperature, magnetic induction, electromotive force, electric current, capacitor charge, output power

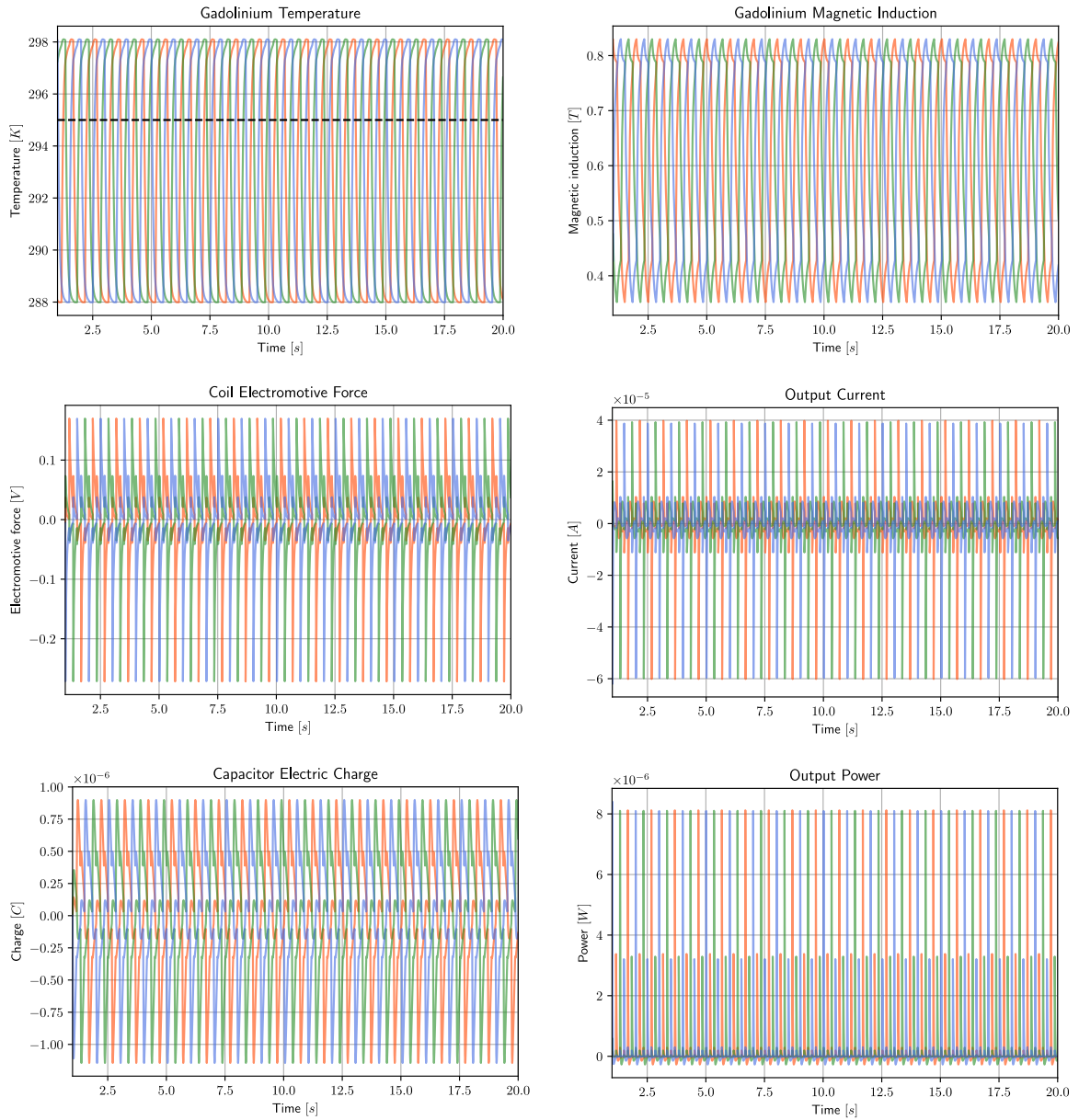


Figure 8. Long time scale graphs of (left to right, top to bottom) temperature, magnetic induction, electromotive force, electric current, capacitor charge, output power

heat exchanger liquid and gadolinium $K = 160 \text{ W/K}$, one gadolinium bar cross section area $A_{\text{Gd}} = 4 \text{ cm}^2$, permanent magnet remanence $B_r = 1.4 \text{ T}$, permanent magnet cross section area $A_{\text{mag}} = 4 \text{ cm}^2$, number of coil loops $N_{\text{coil}} = 100$, coil resistance and load resistance $R_{\text{coil}} = R_{\text{load}} = 2000 \Omega$, load capacitance $C_{\text{load}} = 1 \times 10^{-5} \text{ F}$.

Three gadolinium bars were used (so $N_{\text{Gd}} = 3$), this configuration was selected because it is the most complex and allows for the observation of the greatest number of effects. The simulation lasted $t = 20 \text{ s}$, time step $\Delta t = 1 \times 10^{-3} \text{ s}$, liquid swap frequency in each heat exchanger $f = 1 \text{ Hz}$, cold and hot liquid temperatures are respectively $T_C = 288 \text{ K}$ and $T_H = 298 \text{ K}$. The resulting final oscillation graphs can be seen in figure 7. Here, each colour represents different gadolinium bar. In total, three bars, so three colours: red, green and blue.

Temperature graphs (top-left in figure 7) seem to be close to piecewise exponential as temperature approaches temperature of the liquid currently interacting with the corresponding gadolinium bar. The perturbations from exponential behaviour (most clearly seen when temperature approaches maximum) are explained by magnetocaloric effect: note that these perturbations correspond to dramatic changes in magnetic field distribution (see below). It can also be seen, that these perturbations result in temperatures reaching slightly beyond expected maximum (about 0.1 K higher, quite noticeable) and minimum (0.01 K lower, much smaller) temperatures, which is impossible without outside power input due to second law of thermodynamics, therefore negative power output occurring during this time is expected.

Magnetic induction graph (top-right in figure 7) can be separated into six sections. First, just after 19 s mark blue bar magnetic induction starts increasing, at the same time red and green bars are experiencing decrease in magnetic induction due to redistribution of magnetic field between all bars; the reason is rapid decrease of blue bar temperature which increases its magnetic permeability. Second, just after 19.2 s mark, blue bar magnetic induction has completed rapid increase stage, and red bar magnetic induction starts dropping while green and blue bar magnetic inductions start to increase; this is explained by rapid increase of red gadolinium bar temperature which reduces its magnetic permeability. The same pattern repeats itself for every "bar colour combination", the pattern occurs due to set phase shift of 120° between gadolinium bar temperatures.¹

Electromotive force graph² (centre-left in figure 7) reveals tall peaks whenever a transition between hot and cold liquids occurs in any heat exchanger. Negative electromotive force peaks are noticeably taller, while positive electromotive force peaks are wider; this is explained by asymmetrical temperature behaviour in relation to Curie temperature (see top-left graph

¹In fact, phase shift affects only which liquid is currently in the heat exchangers, which has a direct connection to gadolinium bar temperature functions.

²The electromotive force data itself is useful because it closely resembles voltage data we would get from the generator if the circuit is open.

in figure 7, Curie temperature is represented by black dashed line). During the decrease temperature goes through Curie temperature region rapidly resulting in higher but thinner peaks. During the increase temperature goes through Curie temperature region slower, resulting in shorter but wider peaks. The most optimal temperature range is discussed later in this section. Smaller peaks correspond to change in magnetic flux due to redistribution of magnetic field between all gadolinium bars when temperature of one of them changes.

Electric current graph (centre-right in figure 7) strongly correlates with electromotive force graph. The discrepancies can be explained by non-zero inductance and capacitance in the circuit. Additionally, we can observe that electric current graphs seem to resemble analytical solution of equation 3.9 — dampened oscillation, where inductance and capacitance cause the oscillation, and resistance causes dampening.

Capacitor charge graph (bottom-left in figure 7) shows oscillations around neutral charge, which is an expected result. The capacitor charge is entirely defined by electric current and is not used in further calculations.

Output power graph (bottom-right in figure 7) reveals tall thin and short wide peaks, as expected from electromotive force graph (see above). Additionally, it can be seen that power reaches values below zero after the peaks. This was expected because of temperature reaching normally unreachable values: this is power drained from the circuit that causes magnetocaloric effect in the gadolinium bars by affecting the magnetic field with electric current. Here, it can also be seen that effective voltage $U_{\text{eff}} = 29.6 \text{ mV}$, and effective power output $P_{\text{eff}} = 155 \text{ nW}$ on every load resistance R_{load} .

Long time scale graphs are presented in figure 8. It can be seen, that convergence to some periodic behaviour takes place, all recorded parameters seem to be already in an unchanging oscillation pattern from the beginning of the plotting at $t = 1 \text{ s}$. It is reasonable to suggest, that this pattern would continue indefinitely beyond the 20 s mark (at which the simulation was stopped), therefore the system is in equilibrium oscillational state.³

4.2 Series Simulation Results

First series graph example is based on a generator with one gadolinium bar (so $N_{\text{Gd}} = 1$), with each simulation time $t = 2 \text{ s}$, time step $\Delta t = 2 \times 10^{-3} \text{ s}$, and liquid swap frequency $f = 10 \text{ Hz}$. The liquid temperatures are changing parameters between each individual simulation: cold liquid temperature increases $280 \text{ K} \leq T_{\text{C}} \leq 292 \text{ K}$ and hot liquid temperature decreases $306 \text{ K} \geq T_{\text{H}} \geq 294 \text{ K}$. A total of 24 simulations is completed, so the temperature step in both cases is $T_{\text{step}} = 0.5 \text{ K}$. Hot and cold liquid temperature difference is plotted on

³Note that the long time scale graphs are meant to only show discrepancies in data over longer period of time and are not meant to be used as a source of data points: that's what final oscillation (short) graphs are for.

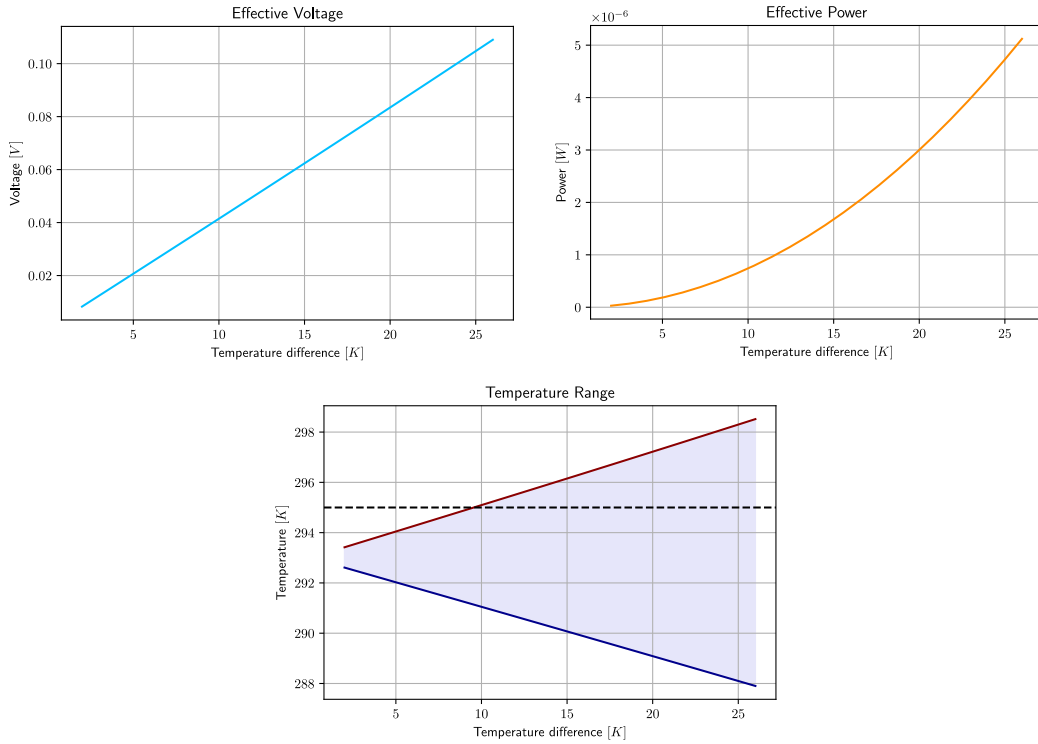


Figure 9. Series graphs of (left to right, top to bottom) output voltage, output power, temperature range against heat exchanger liquid temperature difference

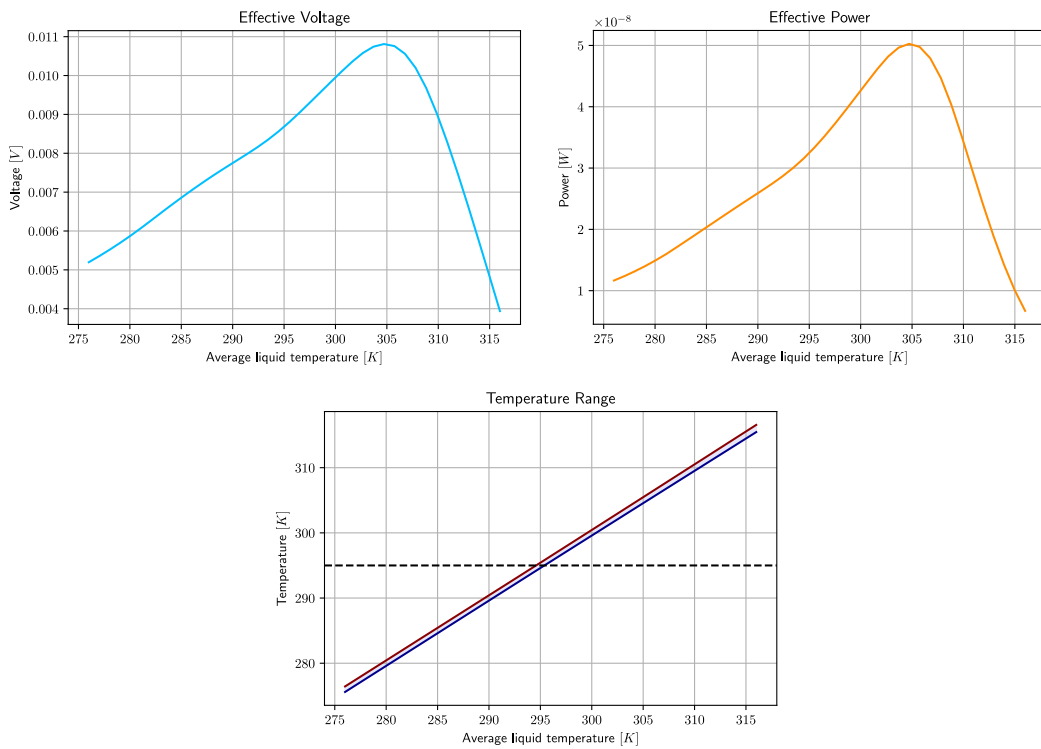


Figure 10. Series graphs of (left to right, top to bottom) output voltage, output power, temperature range against average heat exchanger liquid temperature

the x -axis.

The results can be seen in figure 9. Here, the first graph (top-left) shows output voltage on the load resistance. The voltage seems to be following a linear relation to the temperature difference between hot and cold liquids ΔT . This relation is close to linear when temperature oscillates near Curie temperature, and the difference ΔT is small enough, otherwise a more complex relation is observed. The second graph (top-right) shows power output on the load resistance. Since $P \propto UI \propto U^2$, the graph follows a parabola. Again, this relation only occurs at low ΔT near Curie temperature. Finally, the third graph (bottom) shows maximum and minimum temperature of gadolinium, as well as highlights temperature range, Curie temperature is shown as a black dashed line for reference. It can be observed that gadolinium temperature does not ever reach either liquid temperatures, but the relation between maximum and minimum temperatures and liquid temperature difference ΔT stays linear.

Second series graph example is again covering changing temperature ranges, this time however temperature difference ΔT is constant, and the temperature range is shifted, so that average of hot and cold liquid temperatures changes and can be plotted on the x -axis. The parameters are: number of gadolinium bars $N_{\text{Gd}} = 1$, simulation time $t = 2$ s, time step $\Delta t = 2 \times 10^{-3}$ s, and liquid swap frequency $f = 10$ Hz; cold liquid temperature increases $275 \text{ K} \leq T_{\text{C}} \leq 315 \text{ K}$ and hot liquid temperature increases $277 \text{ K} \leq T_{\text{H}} \leq 317 \text{ K}$, the liquid temperature difference in every case is $\Delta T = 2 \text{ K}$. A total of 40 simulations are completed.

The results can be seen in figure 10. Firstly, it can be seen that both voltage and power peak at average liquid temperature $T_{\text{avg}} \approx 305 \text{ K}$. The heat capacitance graph in figure 6 shows that this region indeed corresponds to one of the strongest magnetocaloric effects.⁴ Additionally, a barely noticeable difference in gadolinium temperature range can be observed in temperature graph (bottom) in figure 10. This difference can be found from numerical data: gadolinium temperature range in the beginning is $\Delta T_{\text{Gd}} = 0.85 \text{ K}$, which later drops to $\Delta T_{\text{Gd}} = 0.81 \text{ K}$ in the centre section of the graph, and then raises up to $\Delta T_{\text{Gd}} = 1.10 \text{ K}$ in the end; this effect can be explained by changing heat capacitance of gadolinium, it is highest in the centre section of the graph at $T_{\text{avg}} \approx 290 \text{ K}$, so gadolinium thermal inertia is higher; the opposite is true for beginning and end of the graph at $T_{\text{avg}} \lesssim 280 \text{ K}$ and $T_{\text{avg}} \gtrsim 300 \text{ K}$.

4.3 Optimization of Parameters

To save space and time, the following list of parameters will be used in the following two sections unless told otherwise:⁵

⁴The area between yellow and orange lines up to the temperature point of interest in the figure 6 is important for magnetocaloric effect.

⁵Parameters were chosen mostly arbitrarily for demonstration purposes (for a "real life" application practical experiments are required), however their values fall within realistic ranges.

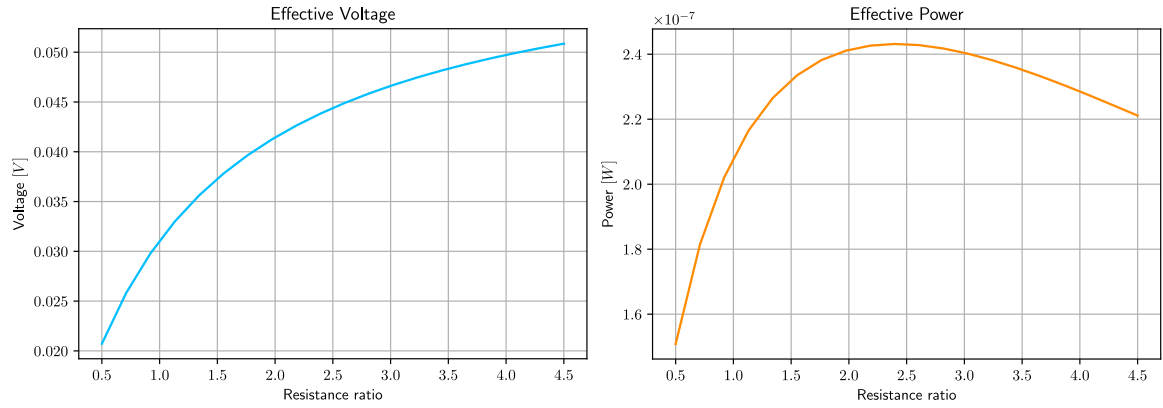


Figure 11. Series graphs of (left to right) output voltage, output power against resistance ratio

- Distance between generator plates $h = 1$ cm;
- Area of one gadolinium bar cross section area $A_{Gd} = 4$ cm²;
- One ferromagnetic plate air contact surface area $A_{air} = 16$ cm²;
- Permanent magnet cross section area $A_{mag} = 4$ cm²;
- Heat transfer parameter between heat exchanger liquid and gadolinium $K = 160$ W/K;
- Permanent magnet remanence $B_r = 1.4$ T;
- Number of coil loops $N_{coil} = 100$;
- Coil resistance and load resistance $R_{coil} = R_{load} = 2000$ Ω;
- Load capacitance $C_{load} = 1 \times 10^{-5}$ F;
- Liquid swap frequency in each bar $f = 2$ Hz;
- Cold and hot liquid temperatures are respectively $T_C = 290$ K and $T_H = 300$ K;
- Number of gadolinium bars $N_{Gd} = 1$;
- Number of simulations in series $N_{sim} = 20$;
- Simulation time $t = 2$ s;
- Time step $\Delta t = 1 \times 10^{-3}$ s.

Before anything else, it is reasonable to take a look at simpler parameters.

1. **Resistance ratio** $\frac{R_{load}}{R_{coil}}$. It is known that in case of a conventional generator this ratio should be equal to one to optimize power output: smaller ratio would reduce the output voltage on the generator load, higher ratio would reduce the electric current in the circuit, their product should be maximized as seen from equation 1.33. It is reasonable to expect that the same will be the case for gadolinium generator. For the testing of this hypothesis, coil resistance $R_{coil} = 2000$ Ω = const; while load resistance will change from $R_{load} = 1000$ Ω to $R_{load} = 9000$ Ω.

The results can be seen in figure 11. From the graphs it is visible that one-to-one ratio is in fact not optimal under specified conditions, the ratio that optimizes power output under these conditions is $\frac{R_{load}}{R_{coil}} \approx 2.4$. Otherwise, the graphs follow the expected

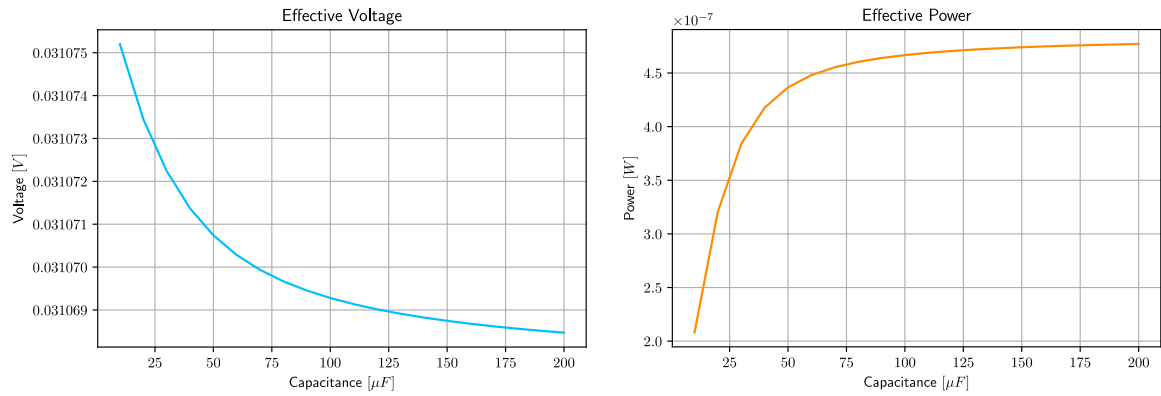


Figure 12. Series graphs of (left to right) output voltage, output power against load capacitance

pattern. The difference probably arises from other electric components of the circuit introducing additional impedance, abnormal behaviour of electromotive force in the generator might exacerbate the effect as well.

2. **Load capacitance** C_{load} . The optimal value in this case is heavily dependent on coil inductance and can be approximated using alternating current formulae. However, this method is questionable due to abnormal behaviour of electromotive force: it can hardly be assumed to be sinusoidal which an assumption of alternating current formulae. If the current was sinusoidal, we could expect some optimal capacitance value that would maximize power output. The capacitance in the series simulation changes from $C_{load} = 10 \mu F$ to $C_{load} = 200 \mu F$.

The results can be seen in figure 12. Voltage changes are marginal, however output power increase is noticeable. It seems that the power output levels out at higher capacitances; this means that a capacitor is not needed in the circuit.⁶ This can be explained by changing self-inductance of the coil: initially capacitor is introduced to compensate coil self-inductance, however the capacitance range that results in improvements is small at a constant self-inductance; since the self-inductance changes with change in gadolinium properties, no one capacitance value could be beneficial during whole time of generator work.

3. **Self-inductance of the coil** L_{coil} . As mentioned earlier, self-inductance itself is not constant during the simulation. However, it is heavily tied to number of coil loops, so this will be the tested parameter. The number of coil loops in the series simulation changes from $N_{coil} = 10$ to $N_{coil} = 200$. The resistance does not change, so we assume that wires of different cross section areas are used. Then, it is reasonable to expect increase in power output when number of coil loops is increased.

The results can be seen in figure 13. The relation between voltage and number of coil loops is linear, as the theory predicts (see equation 3.8). Therefore, number of coil loops has to be maximized, as expected.

⁶Since the capacitor is connected in series, a conductive wire is equivalent to a capacitor with infinite capacitance.

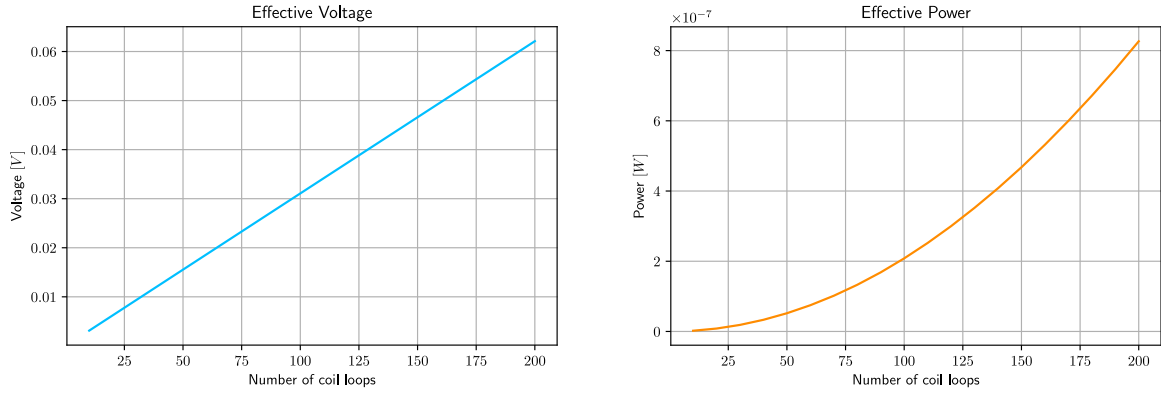


Figure 13. Series graphs of (left to right) output voltage, output power against number of coil loops

- Generator frequency f .** Higher frequencies increase average power output by increasing frequency of power peaks. However, higher frequencies also decrease temperature difference between minimum and maximum temperatures of gadolinium bars, which in turn reduces power output. So, there are two combating effects. A range of frequencies between $f = 2$ Hz and $f = 21$ Hz is used in the simulation.⁷

Results can be seen in figure 14. As foretold, temperature range decreases, while power output increases due to more frequent peaks. The effects seem to reach equilibrium state when frequency reaches $f = 15$ Hz, and output power and voltage reach plateau. Some noisy behaviour is clearly visible, it is probably the effect of multiple (imperfect) numerical methods being used resulting in error accumulation.

- Number of gadolinium bars N_{Gd} .** As a reminder, up to three bars are allowed, each of which heats and cools with constant phase shift relative to others. To compare them and find out whether this phase shift is beneficial, same volume of permanent magnet has to be used per gadolinium bar; this can be achieved by multiplying magnet cross section area by number of gadolinium bars. Other parameters have to be constant. Since there are only three data points, graph plotting is unnecessary.

The results are as follows: single gadolinium bar generator produces power $P_1 = 208$ nW; double gadolinium bar generator produces power $P_2 = 232$ nW per bar; triple gadolinium bar generator produces power $P_3 = 238$ nW per bar. Thus, it can be seen that using multiple bars with phase shift in the same system increases power output. This can be connected to beneficial phase shift, which increases magnetic flux change when it is needed, and creates additional power output peaks. Another possible explanation is connected to generator geometry and magnetic field distribution; it is discussed later in this section.

- Heat conductivity parameter K .** It affects the cooling and heating speed of gadolin-

⁷This range may seem strange: it was chosen due to better convergence of the simulation in this range, otherwise tendencies seem to be unchanged; in fact, the same is true for every range one might consider weird in this section.

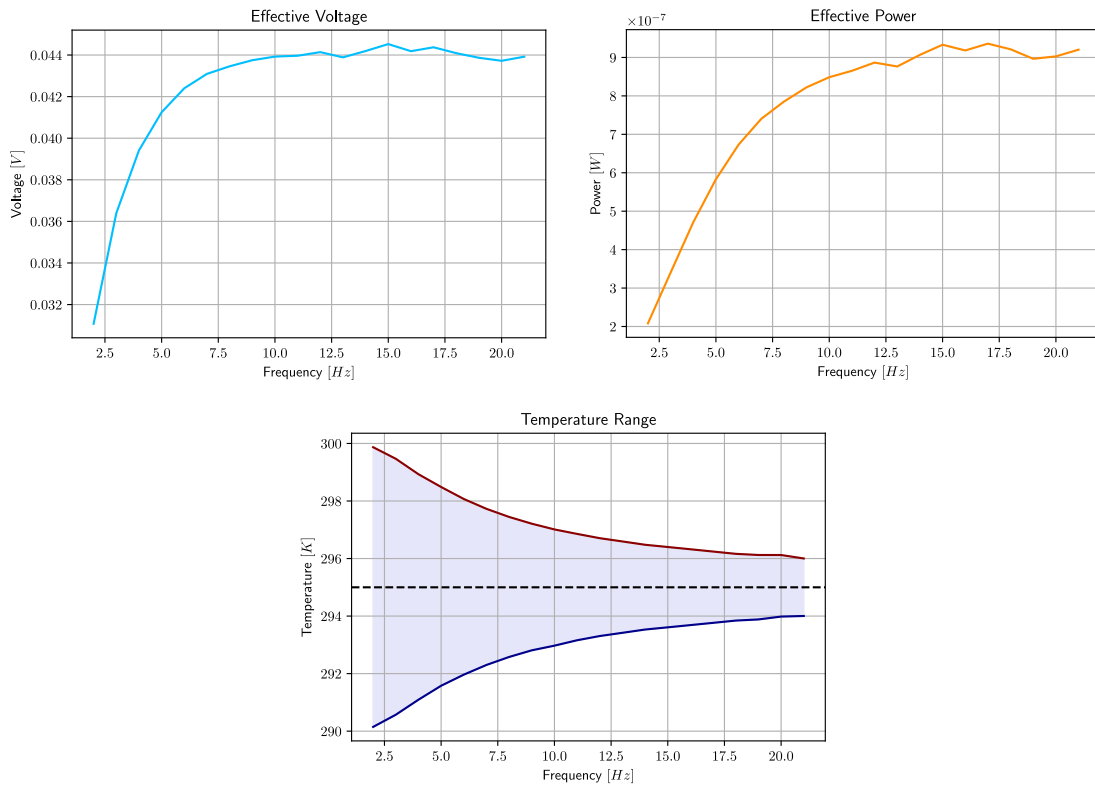


Figure 14. Series graphs of (left to right, top to bottom) output voltage, output power, temperature range against generator frequency

ium. Therefore, with increase of K it is reasonable to expect an increase in output power due to more rapid temperature change. The parameter changes from $K = 20 \text{ W/K}$ to $K = 400 \text{ W/K}$.

The results can be seen in figure 15. As expected, power output increases with increasing heat conductivity parameter K . When temperature amplitude approaches maximum possible value, this relation seem to be linear. Before that, however, increase in voltage is faster.

Permanent magnet remanence B_r . Next, we will take a look at a permanent magnet used in the generator, and generator geometry. The highest currently available value of a permanent magnet remanence $B_r \approx 1.5$, everything lower than that is possible. It is reasonable to expect larger magnetic field to cause higher power output. However, an opposite effect is possible: at too high magnetic fields magnetization difference decreases as seen in figure 6. Remanence is tested in range between $B_r = 1.0$ and $B_r = 2.0$.⁸

The results can be seen in figure 16. One of the earlier described effects is observed: increasing remanence decreases power output. This effect can be explained by looking at heat capacitance

⁸Again, this range may seem strange; additionally, the simulation seems to behave weirdly at lower remanences due to usage of numerical methods; this is considered to be one of the major unsolved problems of this model and is discussed later.

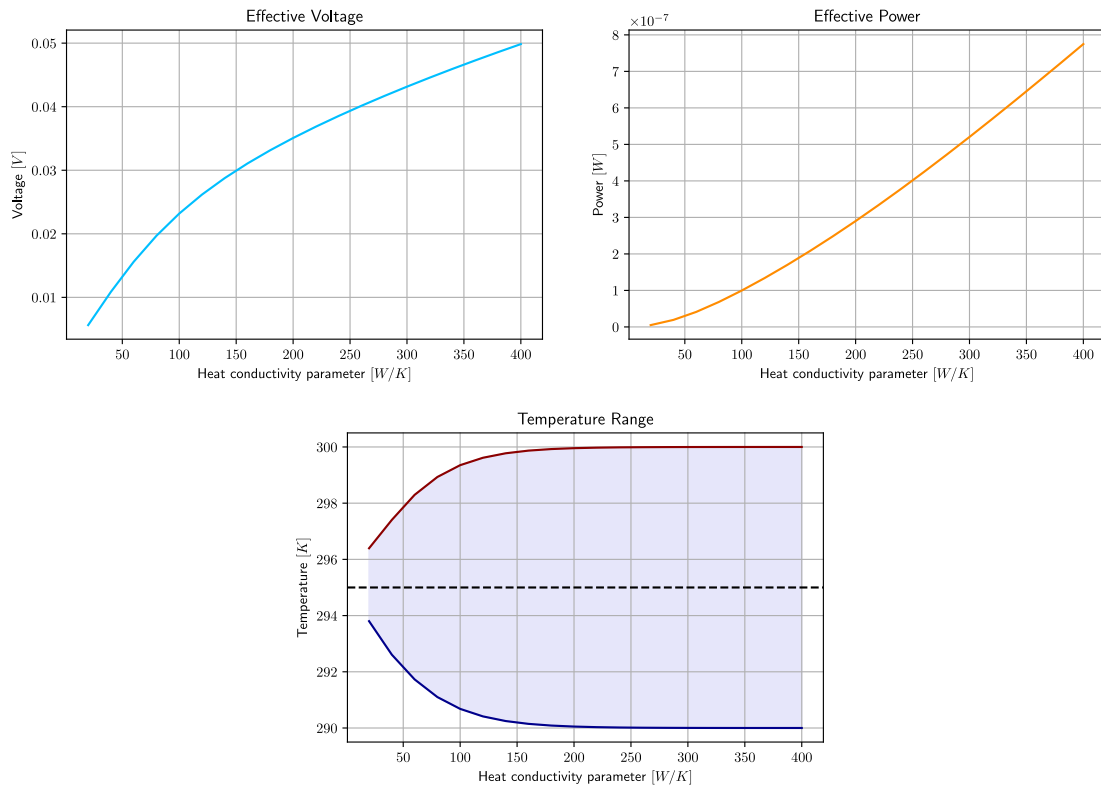


Figure 15. Series graphs of (left to right, top to bottom) output voltage, output power, temperature range against heat conductivity parameter

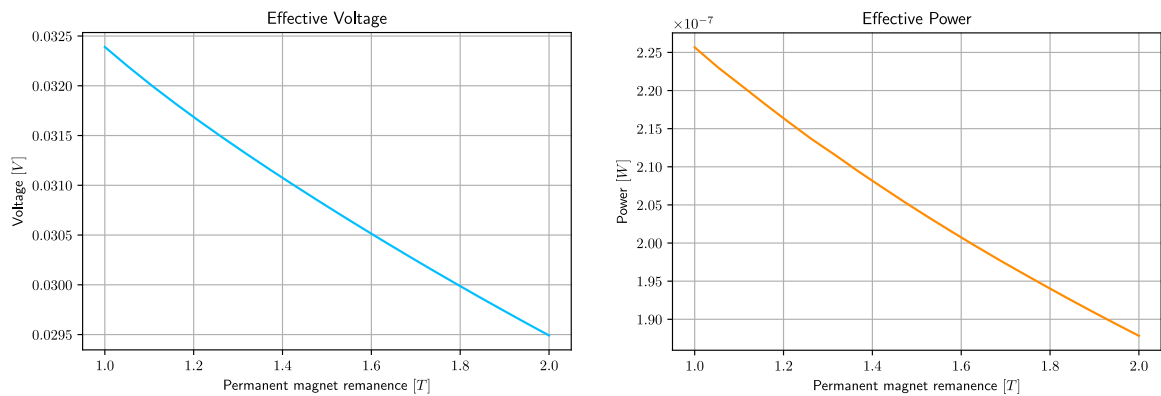


Figure 16. Series graphs of (left to right) output voltage, output power against permanent magnet remanence

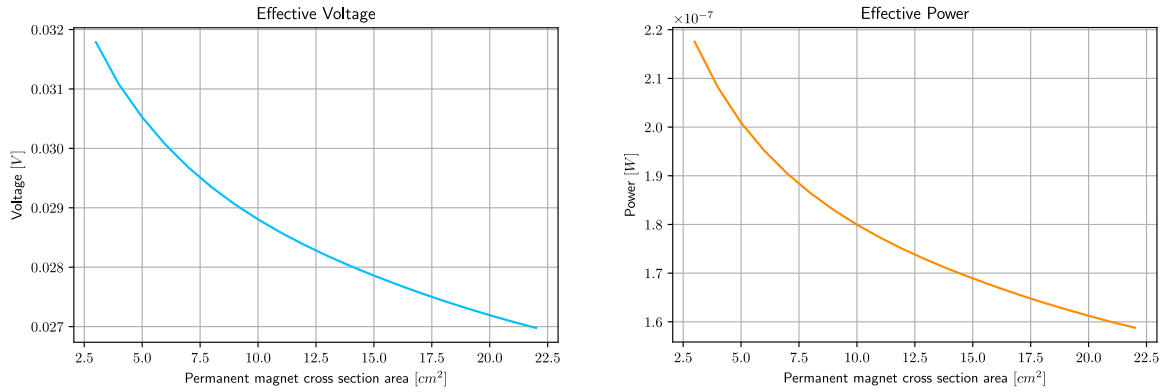


Figure 17. Series graphs of (left to right) output voltage, output power against permanent magnet cross section area

graph in figure 6. The magnetocaloric effect (so the difference between heat capacitance integrals at different magnetic fields over temperature) is the source of energy for the generator. When magnetic field increases, the heat capacitance lines become more densely packed, so the available amount of energy decreases when increasing magnetic induction. In this case, it seems, this effect dominates the other effect (see below), so decrease in power output is observed.

It is also obvious that permanent magnet remanence $B_r = 0$ does not allow any energy production because there is no magnetic field change: it is zero in every generator part. When remanence increases, some variations in magnetic field appear which are proportional to remanence B_r . At weaker magnetic fields this effect should dominate.⁹

Therefore, there must be some optimal permanent magnet remanence, size and other generator parts' geometry, that results in optimal power output. Finding this optimal spot is complicated due to it being affected not only by remanence, but also by generator geometry, and simulation divergent behaviour at weaker magnetic fields.

4.4 Optimization of Geometry

Now, generator geometry parameters are to be investigated.

1. **Permanent magnet cross section area A_{magnet} .** If the previous conclusions are correct, we may expect a decreasing power output when increasing magnet cross-section area under the conditions presented at the beginning of this section. Permanent magnet cross section area changes from $A_{\text{magnet}} = 3 \text{ cm}^2$ to $A_{\text{magnet}} = 22 \text{ cm}^2$.

The results can be seen in figure 17. As predicted, power output decreases with increasing permanent magnet cross section area (and, therefore, increasing magnetic induction in gadolinium). The reasoning is the same as in the case of changing remanence B_r

⁹This effect has not been observed due to divergent behaviour of the simulation; this is discussed in chapter 5.

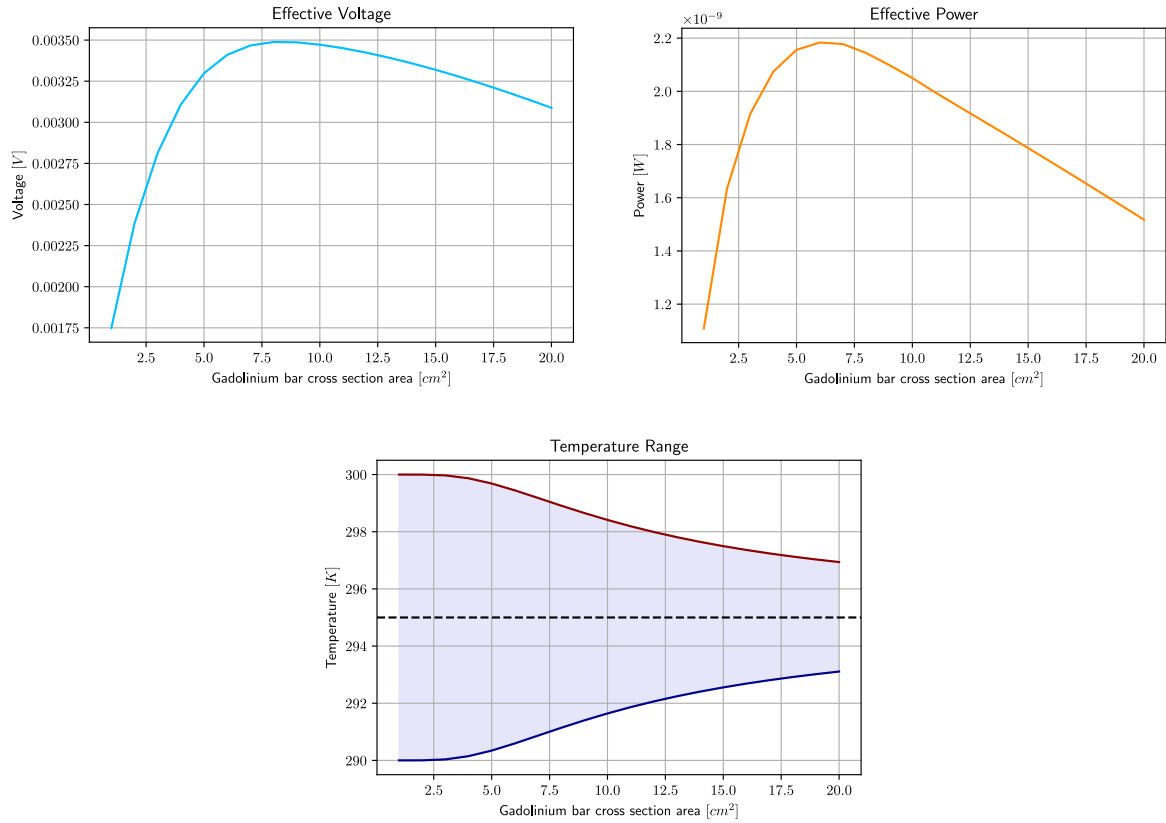


Figure 18. Series graphs of (left to right, top to bottom) output voltage, output power, temperature range against gadolinium bar cross section area

above.

2. **Gadolinium bar cross section area** A_{Gd} . This area is, again, connected to magnetic field distribution. It is reasonable to expect from previous conclusions that the output power will increase up to some optimal cross section area, after which the decrease will be observed: the increase of cross section area increases gadolinium bar heat capacity and slows down temperature change which reduces power output; at the same time the increase of cross section area of a gadolinium bar also decreases magnetic induction, which has been observed to increase power output. Either of these effects could dominate. The selected range is from $A_{Gd} = 1 \text{ cm}^2$ to $A_{Gd} = 20 \text{ cm}^2$. Additionally, number of coil loops is set to ensure convergence: $N_{coil} = 10$.

The results can be seen in figure 18. Power output peaks at $A_{Gd} \approx 6 \text{ cm}^2$, after which increase of thermal inertia of the bar starts to dominate. Before that the increase is explained by the same process as described for remanence above.

3. **Ferromagnetic plate air contact surface area** A_{air} . From the assumptions of the simulation and earlier conclusions, it is expected that larger air contact surface area would allow for higher output power. The range is from $A_{air} = 4 \text{ cm}^2$ to $A_{air} = 80 \text{ cm}^2$. Additionally, number of coil loops is set to ensure convergence: $N_{coil} = 10$.

The results can be seen in figure 19. The results seem reasonable in the context of

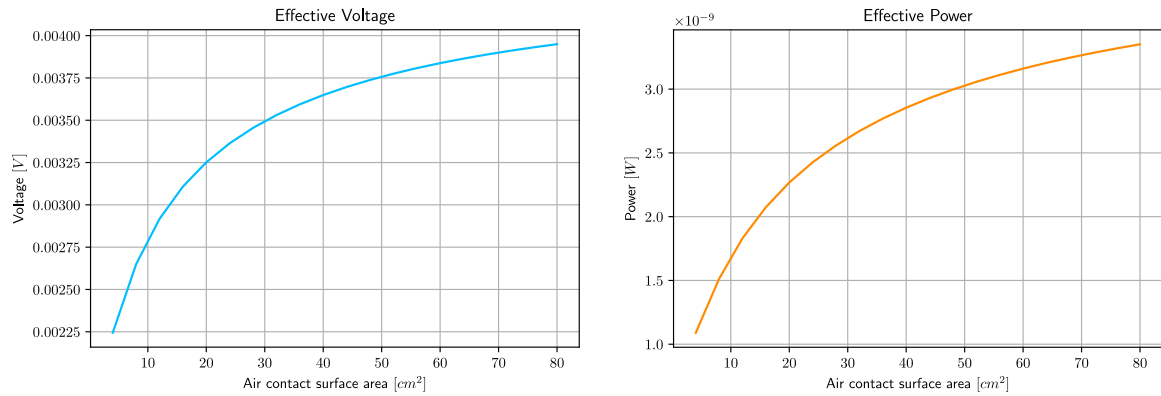


Figure 19. Series graphs of (left to right) output voltage, output power against ferromagnetic plate air contact surface area

assumptions made in chapter 1. In reality, however, ferromagnetic plates do not have infinite magnetic permeability, therefore the output will start to decrease at some point. The initial increase arises from creation of alternative "path" for magnetic field outside of gadolinium, which decreases magnetic induction in gadolinium, which has been observed to increase power output.

4. **Generator height h .** Due to the assumptions, the height should only affect heat capacity of gadolinium bars, thus increasing it should decrease power output. The range is from $h = 2$ mm to $h = 40$ mm.

The results can be seen in figure 20. As expected, increased thermal inertia of gadolinium reduces the amplitude of temperature oscillations, which reduces power output. No other effects are present in the context of assumptions made in chapter 1. However, in reality it can be expected that increased height will additionally increase effective air contact surface area due to magnetic field leaking out. If we assume, that height is much smaller than the other dimensions of the ferromagnetic plates, this effect can be assumed to be negligible.

4.5 Analysis of Optimal Conditions

The results presented in the previous section can now be evaluated. Note that these evaluations are untested experimentally and, therefore, are largely speculative.

- **Distance between generator plates h** is one of the less interesting parameters due to the assumptions of the model.

It has been assumed in chapter 1 that magnetic field lines between the ferromagnetic plates are always perpendicular to the plates. In reality, magnetic field distribution is much more complex.

The generator height h does not affect number of coil loops, or magnetic field distribution in other ways than change of thermal inertia: permanent magnet size and

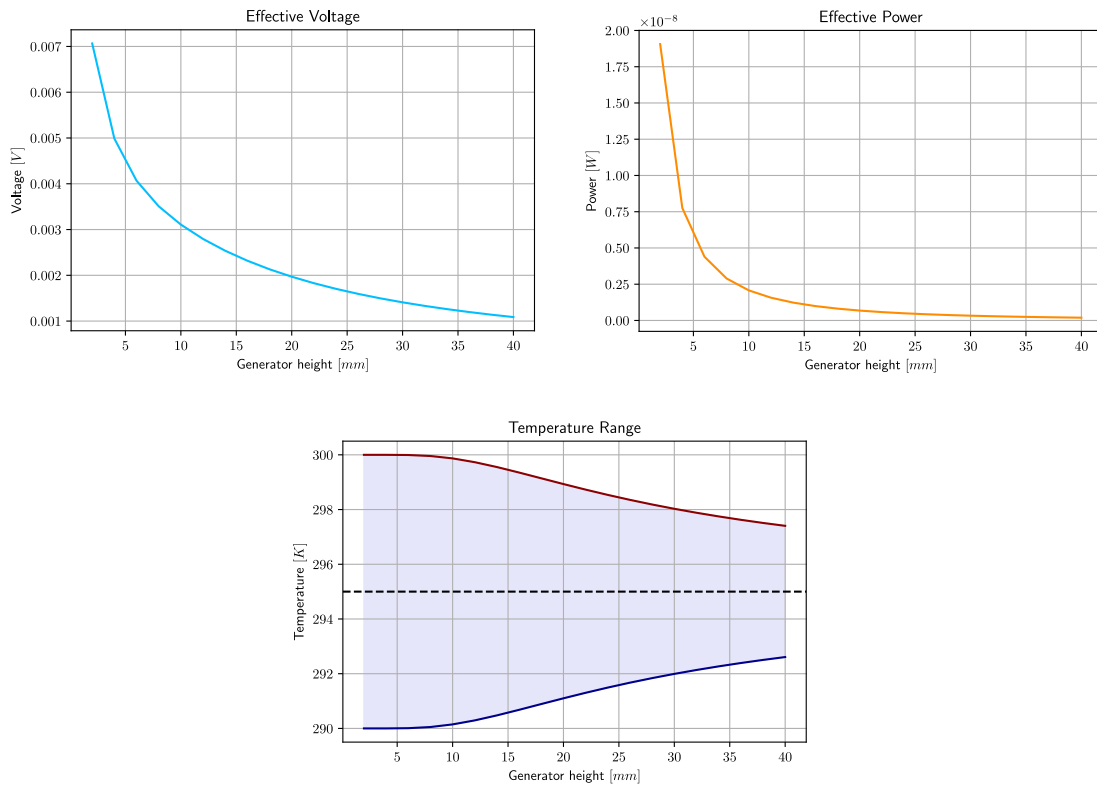


Figure 20. Series graphs of (left to right, top to bottom) output voltage, output power, temperature range against generator height (distance between two ferromagnetic plates)

gadolinium bar size are both proportional to the height, so magnetic field distribution does not change in this way due to height change.

The only way height affects results is by affecting gadolinium bar volume $V_{Gd} = A_{Gd}h$, which increases gadolinium bar heat capacity proportionally to height. However, heat transfer parameter K is not increased automatically, so more time is required to achieve same temperature change.

In reality, more effects are present. Additionally, depending on generator structure, heat transfer parameter K may increase with height h .

The model is only reliable in case of height $h \ll r$, where r is average linear size of the generator in directions perpendicular to height.

- **Gadolinium bar cross section area** A_{Gd} has been observed to have an optimal value for power output.

The effects of gadolinium bar cross section area increase are as follows: gadolinium bar volume and consequent heat capacity increase; redistribution of magnetic field; increase of coil cross section area and consequent increase of self-inductance.

The effects of magnetic field redistribution are evaluated later in this section with remanence B_r .

The effects of increasing coil cross section area seem to dominate at lower values of A_{Gd} . At higher values, decrease in temperature amplitude caused by higher heat

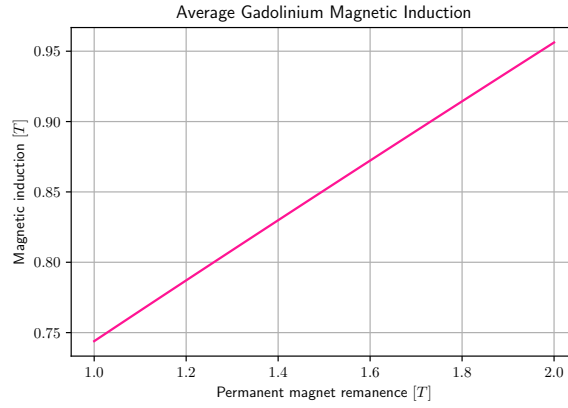


Figure 21. Series graph of average gadolinium magnetic induction against permanent magnet remanence

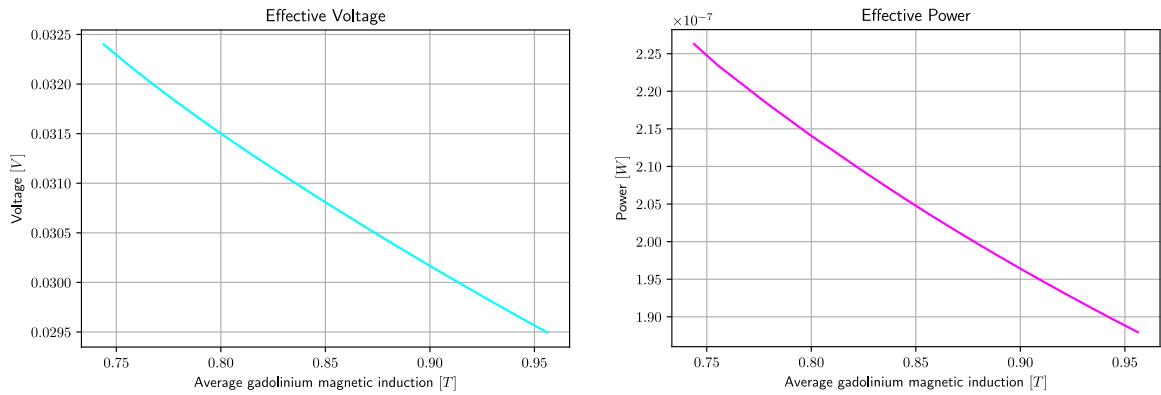


Figure 22. Series graphs of (left to right) output voltage, output power against average gadolinium magnetic induction

capacity with unchanging heat transfer parameter K dominates.

The model seems to predict the behaviour of the generator at different reasonable gadolinium bar cross section areas A_{Gd} well.

- **Ferromagnetic plate air contact surface area** A_{air} is only meaningful in the context of magnetic field distribution, which is discussed separately with remanence B_r .
- **Permanent magnet cross section area** A_{magnet} is, again, only important in the context of magnetic field distribution and is discussed later with remanence B_r .
- **Heat transfer parameter** K has shown predictable behaviour.

Increasing heat transfer parameter K increases heat flux between gadolinium bar and heat exchanger liquid. Faster changing temperature allows to set generator to higher frequencies and to increase temperature amplitude.

Heat transfer parameter K change effects are well predicted by the model.

- **Permanent magnet remanence** B_r is one of the questionably simulated parameters. Permanent magnet cross section area A_{magnet} and remanence B_r affect magnetic field distribution in a similar way: increase in either increases magnetic induction in gadolinium bars. Inversely, increase in ferromagnetic plate air contact surface area A_{air} or

gadolinium bar cross section area A_{Gd} decreases magnetic induction in gadolinium bars.

The first effect, that has clearly been observed: higher fields decrease generator output. The potential explanation is as follows: at higher magnetic fields variations in heat capacitance become smaller (see figure 6). This decrease in variations is more significant than increase in magnetic field amplitude. Since the difference between heat capacitance integrals over temperature of a gadolinium bar at different magnetic fields is the source of energy for the generator, the power output decreases.

While this behaviour has a potential explanation, it seems to be too strong and overall unrealistic.

The second effect: higher magnetic field cause higher magnetic field amplitude, which is directly tied to electricity production (see equation 1.8).

The second effect has not been observed in the simulation, the possible causes of this problem are presented in the summary of this thesis.

Therefore, the simulation is not fit to model effects due to changing: remanence B_r , permanent magnet cross section area A_{magnet} , ferromagnetic plate air contact surface area A_{air} or gadolinium bar cross section area A_{Gd} in the context of magnetic field distribution.

So, another simplified approach can be used to determine optimal magnetic induction in gadolinium. From figure 6 (right side) it can be seen that the largest magnetization difference is at point $B_{Gd} \approx 0.6$ T. Therefore, it is a reasonable conclusion that for maximal output power magnetic induction in gadolinium has to oscillate around the point $B_{Gd} \approx 0.6$ T.

Additional graph of average magnetic induction in gadolinium bar B_{Gd} against permanent magnet remanence B_r is shown in figure 21.¹⁰

Since connection between remanence and gadolinium magnetic induction seems inaccurate, it is useful to plot output power and output voltage against average gadolinium magnetic induction as well. The results based on the same simulation as above can be seen in figure 22.

As stated above, output should decrease when average gadolinium magnetic induction $B_{Gd} \gtrsim 0.6$ T. The opposite effect at weaker magnetic fields cannot be observed using this model due to divergence of the simulation, and unexpected behaviour of magnetic induction at weaker magnetic fields described above.

- **Number of coil loops** N_{coil} is connected to the divergent behaviour of the simulation. At $N_{coil} > 100$ simulation does not converge due to too strong electric currents appearing in the circuit, which change magnetic field and cause fast and unpredictable temperature oscillations due to magnetocaloric effect.

¹⁰Here, parameters are the same as described in the beginning of the previous section, and permanent magnet remanence changes from $B_r = 1$ T to $B_r = 2$ T, $N_{coil} = 10$.

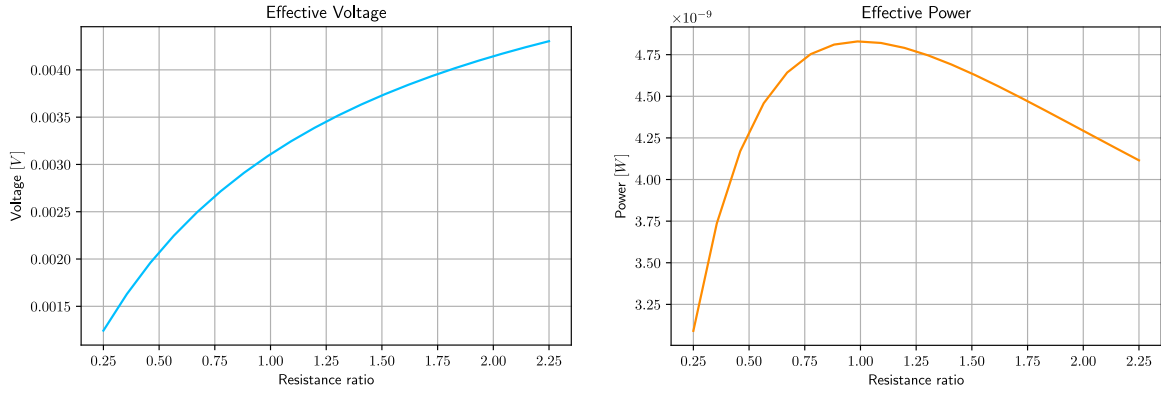


Figure 23. Series graphs of (left to right) output voltage, output power against resistance ratio

Otherwise, the behaviour is expected. Therefore, model is fit for the prediction when $N_{\text{coil}} \leq 100$.

- **Coil resistance** R_{coil} and **load resistance** R_{load} are mostly important in the context of their ratio $\frac{R_{\text{load}}}{R_{\text{coil}}}$.

The behaviour is expected: at a certain resistance ratio power output reaches its maximum. This point might be shifted due to other components in the circuit. This has been confirmed (see figure 23): by setting load capacitance C_{load} to some arbitrary very high value (which is equivalent to no capacitor in the circuit) and number of coil loops $N_{\text{coil}} = 10$ the optimal resistance ratio $\frac{R_{\text{load}}}{R_{\text{coil}}} \approx 1$, which is the expected result.¹¹

Therefore, the model is well fit to simulate power output at different resistances.

- **Load capacitance** C_{load} is used to compensate for generator coil self-inductance. However, the generator coil self-inductance changes during the process of electricity generation due to changing magnetic properties of gadolinium, which suggests that capacitance is not required; this suggestion is supported by the model. This, as well as expected higher impedance at low C_{load} , leads to believe that model is fit to simulate power output with different capacitances C_{load} . However, it is unlikely to be necessary in tested in this thesis generator configuration, since no capacitor circuit is expected to yield the highest power.

- **Liquid swap frequency** f is closely tied to heat transfer parameter K . Similarly, it affects temperature amplitude. Higher frequency means less time for gadolinium to change temperature which reduces power output.

This effect is observed. At higher frequencies some noise tends to appear in the data, however the trend does not change; these perturbations are probably caused by imperfections of numerical methods. Therefore, frequency f is fit to be modelled.

- **Hot liquid temperature** T_{H} and **cold liquid temperature** T_{C} set temperature values to be approached by gadolinium temperature.

¹¹The same simulation parameters were used as in case of resistance ratio calculations in the previous section, except if other values are specified here.

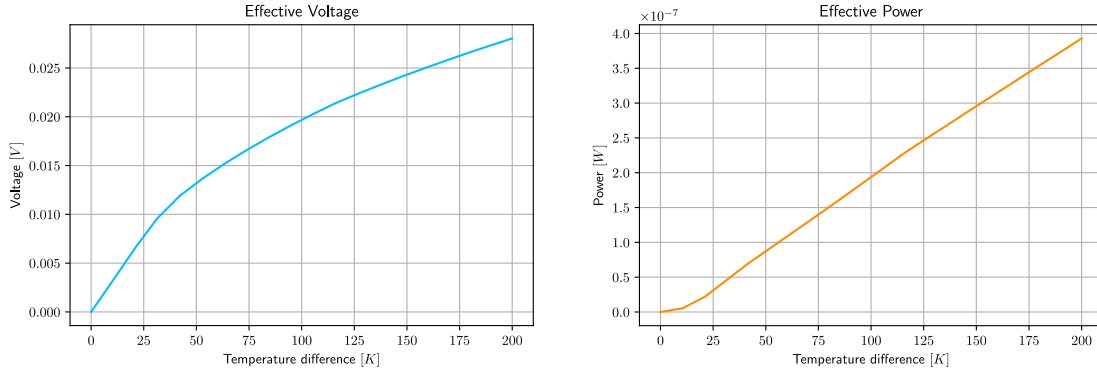


Figure 24. Series graphs of (left to right) output voltage, output power against temperature difference

These two parameters are connected to heat transfer parameter K and liquid swap frequency f . They all show stable and expected behaviour.

It has been found, that temperature range $T_H - T_C$ size is proportional to output voltage when $T_H - T_C \ll T_H$. Otherwise, connection resembling logarithmic function between voltage and temperature difference is observed (see figure 24).

The optimal centre point of the temperature oscillation has been found to be $\frac{T_H + T_C}{2} \approx 305$ K. This seems to be a reasonable result.

Therefore, temperatures T_H and T_C seem to be modelled correctly.

- Number of gadolinium bars N_{Gd} is the main parameter that describes generator configuration.

Its simulation is trivial, no new equations are introduced with this parameter. Therefore, the simulation is entirely dependent on previously discussed parameters at every allowed value of N_{Gd} .

It has been observed, that multiple gadolinium bars in different temperature oscillation phases increase output power per gadolinium bar. This effect is connected to more optimal field redistribution and favourable additional electromotive force peaks in every gadolinium bar in the system during change of magnetic flux in just one of them.

4.6 Results in Optimal Conditions

After finding and evaluating trustworthiness of the optimal parameters it is possible to run the simulation under more optimal conditions.

The conditions are:

- Distance between generator plates $h = 5$ mm;
- Area of one gadolinium bar cross section area $A_{Gd} = 6$ cm²;
- One ferromagnetic plate air contact surface area $A_{air} = 40$ cm²;
- Permanent magnet cross section area $A_{mag} = 4$ cm²;

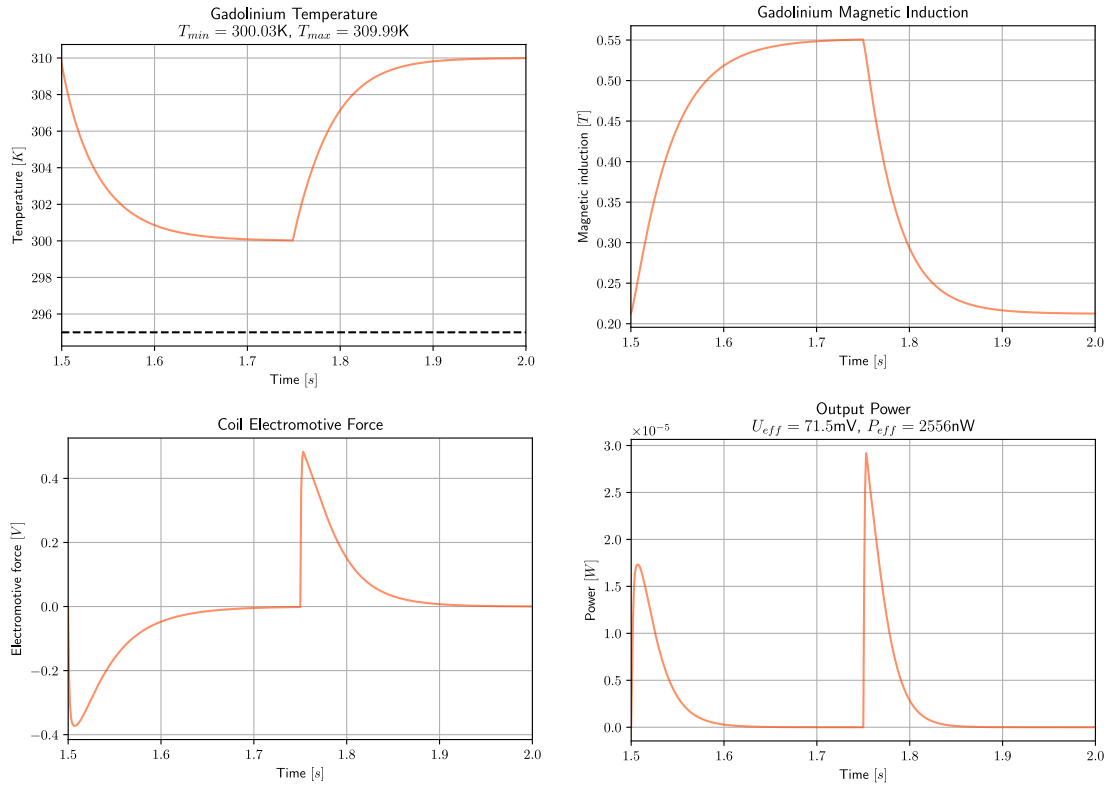


Figure 25. Graphs of (left to right, top to bottom) gadolinium bar temperature, magnetic induction in gadolinium bar, electromotive force in the generator coil, output power

- Heat transfer parameter between heat exchanger liquid and gadolinium $K = 160 \text{ W/K}$;
- Permanent magnet remanence $B_r = 1.4 \text{ T}$;
- Number of coil loops $N_{\text{coil}} = 100$;
- Coil resistance and load resistance $R_{\text{coil}} = R_{\text{load}} = 2000 \text{ ohm}$;
- Load capacitance $C_{\text{load}} = \infty$, or no capacitor;
- Liquid swap frequency in each bar $f = 2 \text{ Hz}$;
- Cold and hot liquid temperatures are respectively $T_C = 300 \text{ K}$ and $T_H = 310 \text{ K}$;
- Number of gadolinium bars $N_{\text{Gd}} = 1$;
- Simulation time $t = 2 \text{ s}$;
- Time step $\Delta t = 1 \times 10^{-3} \text{ s}$.

The results are presented in figure 25. Under conditions present in the beginning of previous section (before optimization) the output voltage was $U_{\text{old}} = 31.1 \text{ mV}$ and output power was $P_{\text{old}} = 208 \text{ nW}$. Under optimized conditions presented above simulation yields $U_{\text{opt}} = 71.5 \text{ mV}$ and $P_{\text{opt}} = 2556 \text{ nW}$. That is a 130% increase in output voltage and an 1129% increase in output power.

It should be noted that we are dealing with a multidimensional extremum searching problem, the solution presented above is just a first order approximation of the correct answer.

5. Conclusions

In this chapter, results, possible improvements and applications are discussed, as well as authors evaluation of the work is presented.

5.1 Equations

The equations derived for the purposes of this thesis have been observed to yield realistic and expected results in most cases. The approach of separation of the calculations into multiple components (thermodynamic, magnetic and electric) has been chosen due to multiple benefits: easier to understand mathematics in each separate part, possibility of direct modification of each part of the simulation without affecting the others, and ability to examine each part of the simulation separately if need be. However, this approach has introduced additional computational complexity and convergence uncertainty into the model.

The numerical algorithm used for solving the set of differential equations by this simulation has been found to be unstable in certain cases. To calculate generator state at point $t = t_0 + \Delta t$, state at point $t = t_0$ is used. In some cases this may result in unpredictable oscillations due to rapid changes of one parameter causing even faster changes of the other parameter: feedback loop is observed. Usually, small enough values of time step of the simulation Δt ensure better convergence, however this makes the process much more computationally intensive. In future, more stable algorithms need to be implemented.

The theoretical part of this thesis can be used as a basis for a more accurate model, where a system of differential equations describing the generator as a whole is constructed. Then, the solution of this system of equations can take into account more data points by using higher order differential equation solution methods. This approach would guarantee better convergence and is likely to solve other issues with predictive power of the model developed in this thesis.

5.2 Gadolinium Properties

Data collection and interpolation is another important milestone, however, improvements are possible. As a reminder, bicubic smooth splines were used to interpolate gadolinium heat capacitance and magnetization data. This method was adequate for the purposes of this thesis, however, it has to be revised to achieve better accuracy.

In the research paper [6], gadolinium heat capacitance interpolant consists of two functions which intersect at Curie temperature point. At this point of intersection, the interpolant does

not have to be smooth, however, for the purposes of this thesis, smooth interpolant was used which may introduce deviations from magnetocaloric effect calculations in the research paper [6]. Additionally, the heat capacitance data might not be dense enough in the regions of weak magnetic field $B < 1.0$ T, which results in lower interpolation accuracy in this region.

Numerical processing of the data can be improved. Currently, numerical integration of heat capacitance data results in error accumulation, as seen in figure 6 (bottom-right). Better results can be achieved if integration is done from both sides (from two points $T \ll T_{\text{Curie}}$ and $T \gg T_{\text{Curie}}$, where magnetocaloric effect ΔT would be negligible, so heat capacitance is the same for initial and final magnetic inductions B_0 and B_1).

5.3 Magnetic Field Distribution

One of the biggest issues with the simulation is unexpected behavior at weaker magnetic fields. This behaviour can be partially explained by the effect described in chapter 4: more potential energy is available at weaker magnetic fields with the same magnetic induction variation. However, this effect is unrealistically strong, and, therefore, the model is believed to be unreliable at weaker magnetic fields.

From some additional testing it has been found that the problem is connected to gadolinium magnetization (see figure 6 right side): it is clearly seen that gadolinium magnetization $M_{\text{Gd}} = 0$ when gadolinium magnetic induction $B_{\text{Gd}} = 0$ at all temperatures. Indeed, when magnetization is manually set to zero in magnetization function when $B_{\text{Gd}} = 0$, the unexpected behaviour of the model is not observed. However, when value from magnetization interpolant is used, some non-zero value is returned by the interpolant at $B_{\text{Gd}} = 0$ due to rounding errors. It seems that there is an interpolation failure of some sort at point $B_{\text{Gd}} = 0$ and other areas with high density of data points¹ might be the reason for the unexpected behaviour at weaker magnetic fields.

If the above hypothesis is true, the model should be trustworthy at gadolinium magnetic inductions $B_{\text{Gd}} \gtrsim 0.6$ T (may vary depending on temperature), since in these areas magnetization data point density is much sparser.

Another possible explanation for unexpected behaviour at weaker magnetic fields is that the approximations used in this thesis yield highly inaccurate results at weaker magnetic fields. As can be recalled from chapter 1, equation 1.22 has division of magnetization M by magnetic induction B in it. If $B = 0$, $M = 0$ as well. So, we obtain $\frac{M}{B} = \frac{0}{0}$, which is an undefined value. When $M \approx 0$, rounding errors become more likely to cause large change in

¹As seen in figure 6 right side, lines at higher temperatures align at lower values of magnetic induction, as well as all lines converge at $B_{\text{Gd}} = 0$; therefore, data being taken from these high density areas may result in spikes in the interpolant.

the final result. However, additional testing has revealed that unexpected behaviour persists even when inductance magnetic fields (the only place where the above approximation is used in the context of magnetic field distribution) are not accounted for, so there must be additional factor(s) at play.

The third hypothesis is connected to systems of equations 1.14, 1.17 and 1.19. It is possible that the approach used in this thesis does not work with lower remanences of the permanent magnet; the separation of magnetic field into permanent magnet, self-inductance and mutual inductance fields is the approach in question. Therefore, a review of magnetic field calculation methods is required; the new approach should calculate magnetic field as a whole. If done correctly, it could be a solution to the above approximation imperfections as well: free currents could be accounted for in the Ampère's circuital theorem, which would allow to calculate total field in gadolinium by solving one system of equations.

In reality, the cause is probably a combination of first and third hypotheses, therefore a revision of both interpolation methods and magnetic field distribution equations is required to improve accuracy at weaker magnetic fields.

It is author's educated guess that the problem is analogous to the divergence of the simple iterations equation solution method. In this method, the equation $F(x) = 0$ is rearranged to be in the form $x = f(x)$, then the iterations $x_i = f(x_{i-1})$ should approach the solution so that $i \rightarrow \infty \Rightarrow F(x_i) = 0$.

This method is rarely used due to a strict convergence condition: $\left| \frac{df(x)}{dx} \right| < 1$. If this condition is not fulfilled, the iterations either diverge, or converge to an incorrect solution. In figure 26, the same function is put into two different coordinate planes. On the left, convergence condition is fulfilled near the zero of the function. On the right, the method converges to an incorrect solution due to unfulfilled convergence condition.

In the case of the model developed in this thesis, magnetic field distribution equilibrium has to be reached. A combination of magnetic field distribution equations and magnetization data yields an iteration method, where with each iteration (so with each time step Δt) the system tries to approach equilibrium point, but at weaker magnetic fields it converges to an incorrect equilibrium; an example of such behaviour is demonstrated in figure 26 on the right side.

This claim can be supported by some observations. If magnetization is manually set to zero at $B_{Gd} = 0$, and remanence $B_r = 0$, the system stays in the equilibrium with no magnetic field. If the magnetization is set to any other value in the same conditions, the system is not in equilibrium state initially and, therefore, approaches some false equilibrium at $B_{Gd} \approx 0.5$ T. Additionally, the graphs presented as an example in figure 26 resemble magnetization graphs presented in figure 6, where point $\frac{dM(B)}{dB} = 1$ is somewhere near $B = 0.5$ T, which is the

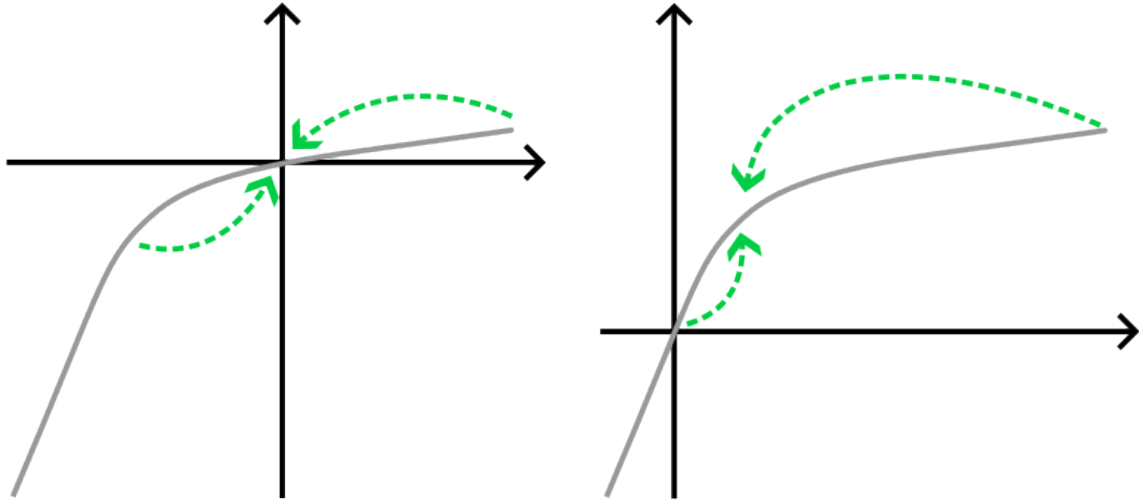


Figure 26. A comparison of unexpected behaviour at weak magnetic fields to simple iterations method: on the left the method yields the correct answer, on the right the method converges to a false answer

false convergence point.

Thus, it seems probable that the effect described above is present in the simulation.

It is also possible that the simulation code contains a mistake that results in unexpected behaviour at low gadolinium magnetic induction values. However, multiple reviews of the magnetic field distribution function in the code has not revealed any mistakes.

5.4 Magnetocaloric Effect

Model excels in magnetocaloric effect calculations. Starting from interpolated data validation, the model has consistently yielded realistic changes of temperature due to magnetic induction change.

In figure 6, magnetocaloric effect was used for interpolation validation purposes. The difference between the measured and the recalculated values was about 10%, due to interpolation imperfections. With interpolation improvements, higher accuracy is possible.

In figure 7, magnetocaloric effect could be observed to be the reason for some temperature changes as described in the corresponding chapter 4. The behaviour is in agreement with calculated negative power output data presented in the same figure 7.

When the divergent behaviour of the simulation was encountered, many parameters such as magnetic induction and electric current entered unpredictable oscillation pattern with enormous amplitudes and frequencies. However, despite that, temperature stayed within reasonable range, with deviations no more than $\Delta T \approx 20$ K, which is an expected limit for

magnetocaloric effect in the context of used interpolated data.

5.5 Evaluation of the Model

The developed model can be used as a basis for more complex models in the future. In this thesis, generator coil was placed around the gadolinium bars. This is, however, not an optimal position. Magnetic field in the gadolinium bar does not change direction, so variations in magnetic induction are relatively small. It is possible to find a place in the generator, where magnetic field does change direction and, thus, increase magnetic field amplitude approximately tenfold [15, 16, 17].

The magnetic field distribution and magnetocaloric effect calculations made in this thesis can be used in other configurations as well with some relatively small modifications.

The model is likely to be applicable for prediction of output power tendencies in changing conditions, as defined in this thesis. To confirm the predictive power of the numerical model, a physical model of the generator has to be built and measured data has to be compared to the predictions.

Magnetocaloric effect calculations, as seen from figure 6, agree with experimentally measured data. Improvements in data interpolation methods would further improve predictive capabilities of the model in terms of magnetocaloric effect.

Electric circuit calculations seem to follow patterns expected from the oscillating current: electromotive force causes the electric current to perform damped oscillations which is expected from the analytical solution of the equation 3.9.

Magnetic field distribution calculations need to be tested experimentally, and new calculation methods have to be introduced. Until then, the predictive power of the model regarding magnetic field distribution serves only as a first approximation.

Acknowledgements

The author would like to thank the following people and organizations:

- Supervisor Jaan Kalda for thesis idea, and providing guidance and feedback throughout the writing of this thesis;
- CAFA Tech OÜ for the direction this thesis took and possibilities of further development;
- Georgi Olentšenko for proofreading and editorial help;
- Karin Olentšenko for proofreading and editorial help.

References

- [1] J. M. Cullen and J. M. Allwood. “Theoretical efficiency limits for energy conversion devices”. In: *Energy* 35 (5) (2010), pp. 2059–2069.
- [2] C. Forman et al. “Estimating the global waste heat potential”. In: *Renewable and Sustainable Energy Reviews* 57 (2016), pp. 1568–1579.
- [3] C. R. H. Bahl and K. K. Nielsen. “The effect of demagnetization on the magnetocaloric properties of gadolinium”. In: *Journal of Applied Physics* 105 (1) (2009), p. 013916.
- [4] J. F. Elliott, S. Legvold, and F. H. Spedding. “Some Magnetic Properties of Gadolinium Metal”. In: *Phys. Rev.* 91 (1) (1953), pp. 28–30.
- [5] F. Darnell and W. Cloud. “Magnetization of Gadolinium near Its Curie Temperature”. In: *Journal of Applied Physics (U.S.)* 35 (1964).
- [6] S. Dan’kov et al. “Magnetic phase transitions and the magnetothermal properties of gadolinium”. In: *Physical Review B* 57 (1998), pp. 3478–3490.
- [7] D. C. Douglass et al. “Magnetic properties of free cobalt and gadolinium clusters”. In: *Phys. Rev. B* 47 (19) (1993), pp. 12874–12889.
- [8] S. P. Mathew et al. “Magnetic irreversibility, spin-wave excitations and magnetocaloric effect in nanocrystalline Gadolinium”. In: *Journal of Physics: Conference Series* 200 (7) (2010), p. 072047.
- [9] T. Gottschall et al. “Magnetocaloric effect of gadolinium in high magnetic fields”. In: *Phys. Rev. B* 99 (13) (2019), p. 134429.
- [10] A. Waske et al. “Magnetocaloric materials for refrigeration near room temperature”. In: *MRS Bulletin* 43 (4) (2018), pp. 269–273.
- [11] R. A. Kishore and S. Priya. “A review on design and performance of thermomagnetic devices”. In: *Renewable and Sustainable Energy Reviews* 81 (2018), pp. 33–44.
- [12] J. F. Elliott. “Thermomagnetic Generator”. In: *Journal of Applied Physics* 30 (11) (1959), pp. 1774–1777.
- [13] T. Christiaanse and E. Brück. “Proof-of-Concept Static Thermomagnetic Generator Experimental Device”. In: *Metallurgical and Materials Transactions E* 1 (1) (2014), pp. 36–40.
- [14] D. Nguyen Ba et al. “Magnetocaloric Effect in Flexible, Free-Standing Gadolinium Thick Films for Energy Conversion Applications”. In: *Phys. Rev. Appl.* 15 (6) (2021), p. 064045.

- [15] A. Waske et al. “Energy harvesting near room temperature using a thermomagnetic generator with a pretzel-like magnetic flux topology”. In: *Nature Energy* 4 (1) (2018), pp. 68–74.
- [16] X. Liu et al. “High-performance thermomagnetic generator controlled by a magnetocaloric switch”. In: *Nature Communications* 14 (1) (2023), p. 4811.
- [17] P. Baliozian et al. “Concept of a Magnetocaloric Generator with Latent Heat Transfer for the Conversion of Heat into Electricity”. In: *Energy Technology* 10 (3) (2022), p. 2100891.
- [18] L. D. Kirol and J. I. Mills. “Numerical analysis of thermomagnetic generators”. In: *Journal of Applied Physics* 56 (3) (1984), pp. 824–828.
- [19] J. Kalda. *Electromagnetism*. Ed. by E. Leinonen and M. Olentšenko. <https://www.overleaf.com/read/ft rhj r w s k y t f # 3 2 5 4 2 f>. Study material. 2024.
- [20] G. Van Rossum and F. L. Drake. *Python 3 Reference Manual*. Scotts Valley, CA: CreateSpace, 2009.
- [21] C. R. Harris et al. “Array programming with NumPy”. In: *Nature* 585 (7825) (2020), pp. 357–362.
- [22] The pandas development team. *pandas-dev/pandas: Pandas*. <https://doi.org/10.5281/zenodo.3509134>. Version latest. 2020.
- [23] W. McKinney. “Data Structures for Statistical Computing in Python”. In: *Proceedings of the 9th Python in Science Conference*. Ed. by S. van der Walt and J. Millman. 2010, pp. 56–61.
- [24] E. Jones, T. Oliphant, P. Peterson, et al. *SciPy: Open source scientific tools for Python*. <http://www.scipy.org/>. 2001.
- [25] J. D. Hunter. “Matplotlib: A 2D graphics environment”. In: *Computing in Science & Engineering* 9 (3) (2007), pp. 90–95.
- [26] Royal Society of Chemistry. *Gadolinium - Element information, properties and uses | Periodic Table*. <https://www.rsc.org/periodic-table/element/64/gadolinium>.
- [27] J. Kalda. *Thermodynamics*. <https://www.ioc.ee/~kalda/ipho/Thermodyn.pdf>. Study material. 2019.
- [28] A. Rohatgi. *WebPlotDigitizer*. <https://automeris.io/>. visited on 2024-05-20.

Abstract

A thermomagnetic generator — a heat engine that operates based on Faraday's law by heating and cooling a ferromagnetic material around the Curie point — has already been proven as a promising concept [12, 15, 16, 17]. The working principle of the thermomagnetic generator is not complicated, but finding its optimal parameters is not possible without a numerical model and simulations. This is because the solutions to Maxwell's equations depend on the shape and mutual arrangement of the ferromagnetic materials, as well as the electromagnetic and thermal properties of the magnetic materials around the Curie point, which are dependent on temperature and magnetic field in a relatively complex manner.

In this thesis, a numerical model for a thermomagnetic generator based on the magnetic and thermodynamic properties of gadolinium is developed, tested, and the modeling results are analyzed.

The equations used for modeling are derived from the fundamental laws of electromagnetism and thermodynamics [19, 27]. The thermal and electromagnetic characteristics of gadolinium necessary for the simulation are taken from literature [6].

The mathematical model, implemented as a computer code, was tested under realistic initial parameter conditions. Testing showed that the model predicts the magnetocaloric effect well, and the results are consistent with existing studies on the properties of gadolinium [6]. Thus, the objective set in the thesis has been achieved: a numerical model has been created that allows predicting the efficiency of a thermomagnetic generator depending on the device parameters.

However, the model still needs to be refined for more accurate calculations: the spatial distribution of the magnetic field is currently found only approximately in the algorithm; this part of the model is planned to be improved in the future. Another part of the model that can and should be improved is the interpolation methodology for the data points of gadolinium's thermomagnetic characteristics taken from the scientific literature.

Keywords: gadolinium, thermomagnetic generator, magnetocaloric effect, numerical modelling.

Annotatsioon

Termomagnetiline generaator — soojusmasin, mis töötab tänu Faraday seadusele soojendades ja jahutades ferromagnetilist materjali Curie punkti ümbruskonnas — on juba ennast tõestatud kontseptsioon [12, 15, 16, 17]. Termomagnetilise generaatori tööpõhimõte pole keeruline, kuid selle optimaalsete parameetrite leidmine pole võimalik ilma numbrilise mudeli ja simulatsioonideta, sest Maxwelli võrrandite lahendid sõltuvad ferromagnetiliste materjalide kujust ning vastastikusest paiknemisest ning magnetiliste materjalide elektromagnetilistest ja soojuslikest omadused Curie punkti ümbruskonnas, mis sõltuvad temperatuurist ja magnetväljast võrdlemisi keerukal moel.

Käesolevas lõputöös töötatakse välja gadoliiniumi magnetilistel ja termodünaamilistel omadustel põhinev termomagnetilise generaatori numbriline mudel, testitakse seda mudelit ja analüüsitakse modelleerimise tulemusi.

Modelleerimiseks kasutatavad võrrandid on tuletatud elektromagnetismi ja termodünaamika põhiseadustest [19, 27]. Simulatsiooniks vajalikud gadoliiniumi soojuslikud ja elektromagnetilised karakteristikud on võetud artiklist [6].

Arvutikoodina realiseeritud matemaatilist mudelit testiti realistlike lähteparameetrite tingimustes. Testimine näitas, et mudel ennustab magnetkalorilist efekti hästi ja tulemused ühtivad olemasolevate gadoliiniumi omaduste uuringute tulemustega [6]. Seega on lõputöös seatud eesmärk saavutatud: on koostatud numbriline mudel, mis võimaldab ennustada termomagnetilise generaatori efektiivsust sõltuvuses seadme parameetritest.

Täpsemateks arvutusteks on mudelit vaja siiski veel täiustada: magnetvälja ruumiline jaotus on praeguses algoritmis leitud üksnes ligikaudselt; seda mudeli osa on plaanis edaspidi täiendada. Teine mudeli osa, mida saab ja tuleb parendada, on teaduskirjandusest võetud gadoliiniumi termomagnetiliste karakteristikute andmepunktide interpolatsiooni meetodika.

Märksõnad: gadoliinium, termomagnetiline generaator, magnetkaloriline efekt, numbriline modelleerimine.

Appendices

Appendix 1 – Non-Exclusive License for Reproduction and Publication of a Graduation Thesis²

I Mihhail Olentšenko

1. Grant Tallinn University of Technology free licence (non-exclusive licence) for my thesis “Modelling of Thermomagnetic Generator Based on Magnetic and Thermodynamic Properties of Gadolinium”, supervised by Jaan Kalda
 - 1.1. to be reproduced for the purposes of preservation and electronic publication of the graduation thesis, incl. to be entered in the digital collection of the library of Tallinn University of Technology until expiry of the term of copyright;
 - 1.2. to be published via the web of Tallinn University of Technology, incl. to be entered in the digital collection of the library of Tallinn University of Technology until expiry of the term of copyright.
2. I am aware that the author also retains the rights specified in clause 1 of the non-exclusive licence.
3. I confirm that granting the non-exclusive licence does not infringe other persons' intellectual property rights, the rights arising from the Personal Data Protection Act or rights arising from other legislation.

20.05.2024

²The non-exclusive licence is not valid during the validity of access restriction indicated in the student's application for restriction on access to the graduation thesis that has been signed by the school's dean, except in case of the university's right to reproduce the thesis for preservation purposes only. If a graduation thesis is based on the joint creative activity of two or more persons and the co-author(s) has/have not granted, by the set deadline, the student defending his/her graduation thesis consent to reproduce and publish the graduation thesis in compliance with clauses 1.1 and 1.2 of the non-exclusive licence, the non-exclusive license shall not be valid for the period.

Appendix 2 – Extracted Data and Simulation Code

Extracted data used in this thesis, as well as simulation code are available at:

<https://github.com/MikeKerman/Modelling-of-Heat-Exchange-Generator-Based-on-Magnetic-and-Thermodynamic-Properties-of-Gadolinium>.